Electronic Supplementary Information for

1,1'-Bi(2-naphthol-4,5-dicarboximide)s: Blue Emissive Axially Chiral Scaffolds with Aggregation-enhanced Emission Properties

Meng-Ting Chen,[a] Yang Zhang,[a] Myroslav O. Vysotsky,[b] Joachim O. Lindner,[b]
Meng-Hua Li,[a] Mei-Jin Lin,[a]* and Frank Würthner [b]*

[a.] *State Key Laboratory of Photocatalysis on Energy and Environment, College of Chemistry, Fuzhou University, 350116 Fuzhou, China. E-mail: meijin_lin@fzu.edu.cn*

[b.] *Institut für Organische Chemie & Center for Nanosystems Chemistry, Universität Würzburg, Am Hubland, 97074 Würzburg, Germany. E-mail: wuerthner@uni-wuerzburg.de*

Table of Contents:

1. Nuclear magnetic resonance (NMR) spectra S2
2. High-resolution mass spectra (HRMS) S16
3. Single-crystal X-ray diffraction analyses S23
   3.1 Methods and crystal data S23
   3.2 The molecular structure of **4b** S24
4. Chiral HPLC analyses of **6a**, **6b**, **1a**, **1b**, **(R)-1a** S25
5. Absorption, fluorescence and circular dichroism spectral measurements S29
6. Cyclic voltammetry measurements S34
7. Theoretical calculations S36
8. Methanol-water system luminescence measurements S38
9. Luminescence lifetime measurements S39
10. References S43

1. Nuclear magnetic resonance (NMR) spectra

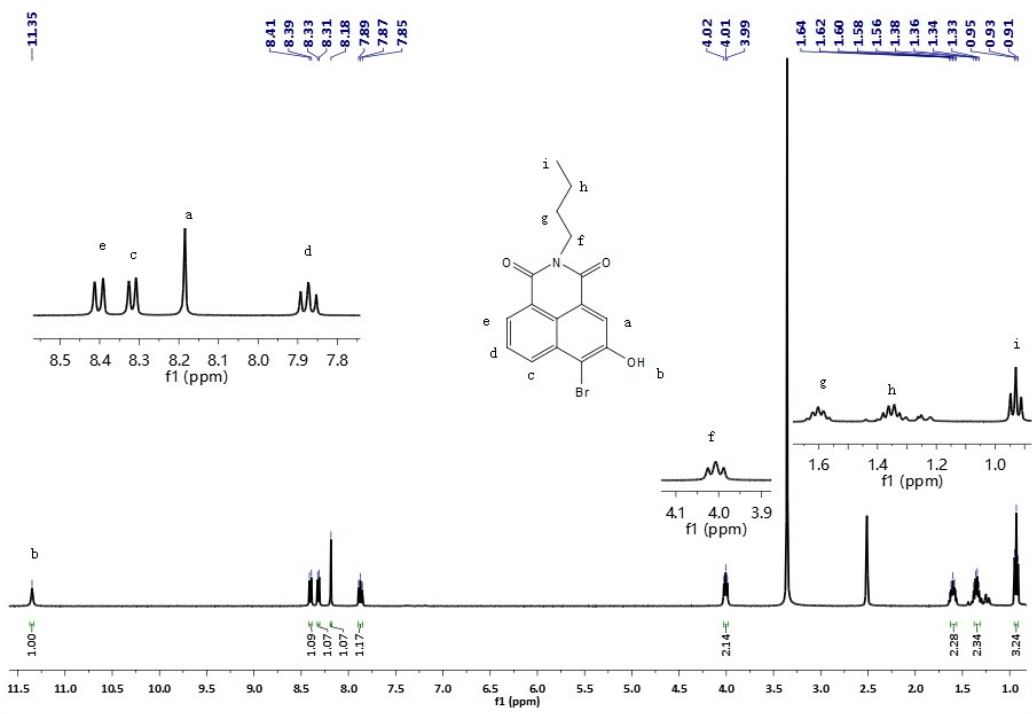

Figure S1. ^{1}H NMR spectrum of **3a** (400 MHz, d_6-DMSO, 298K)

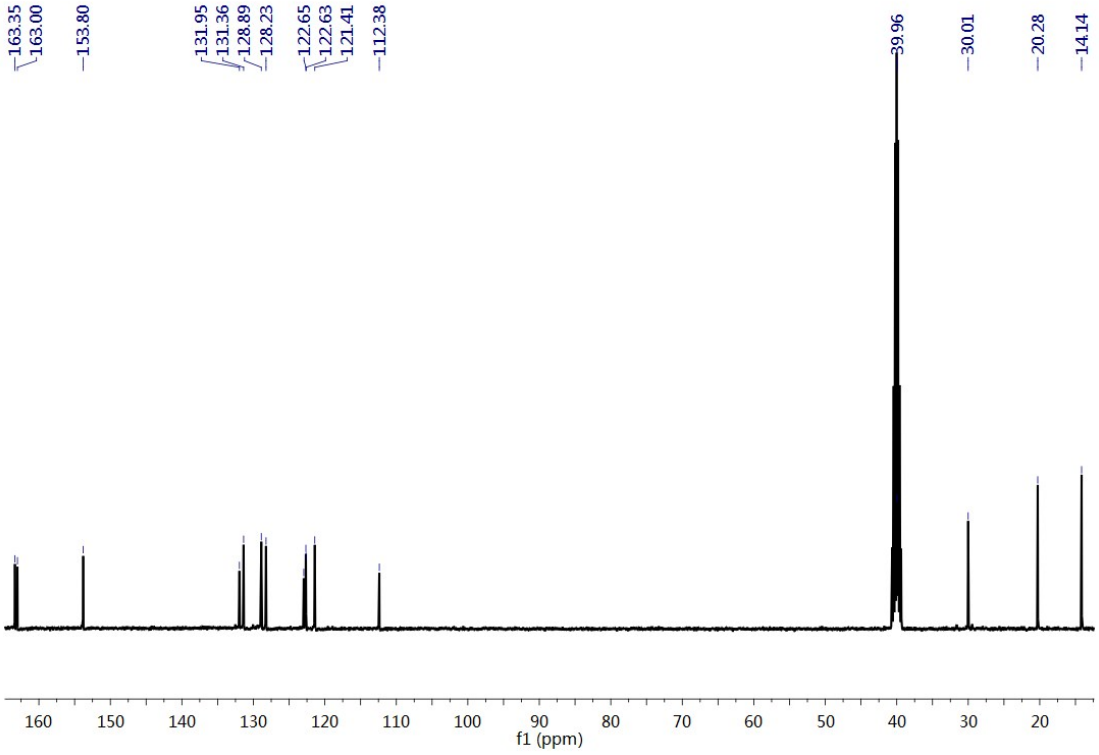

Figure S2. ^{13}C NMR spectrum of **3a** (100 MHz, d_6-DMSO, 298K)

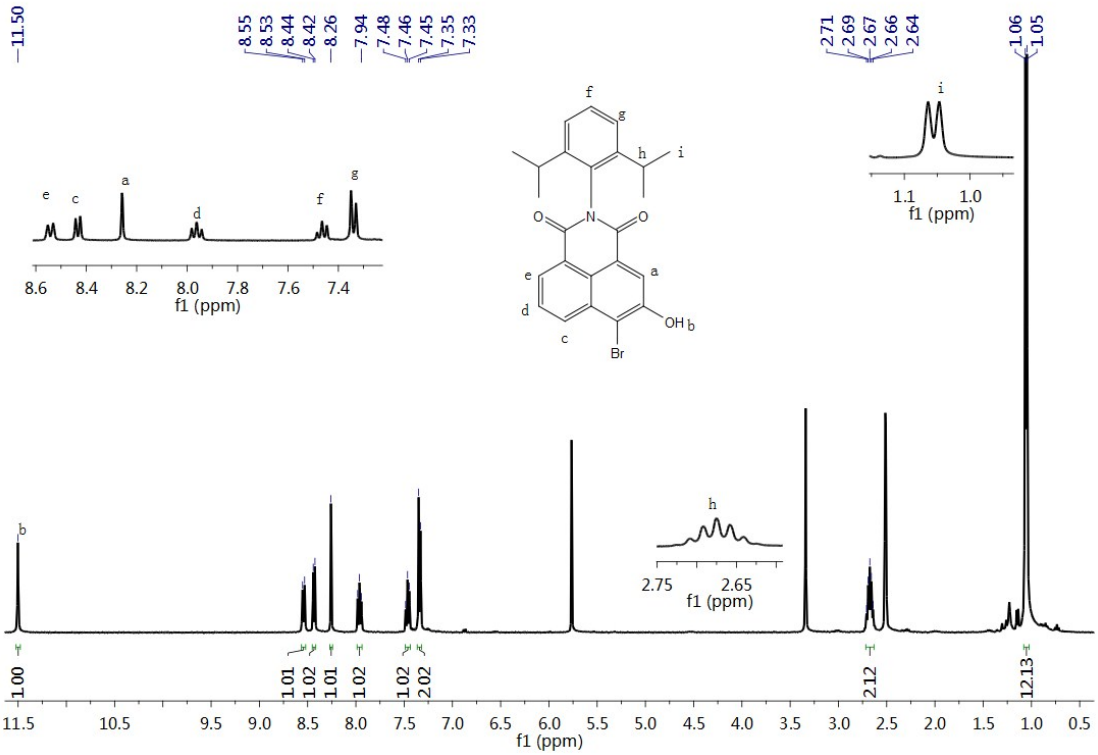

Figure S3. ^{1}H NMR spectrum of **3b** (400 MHz, d_6-DMSO, 298K)

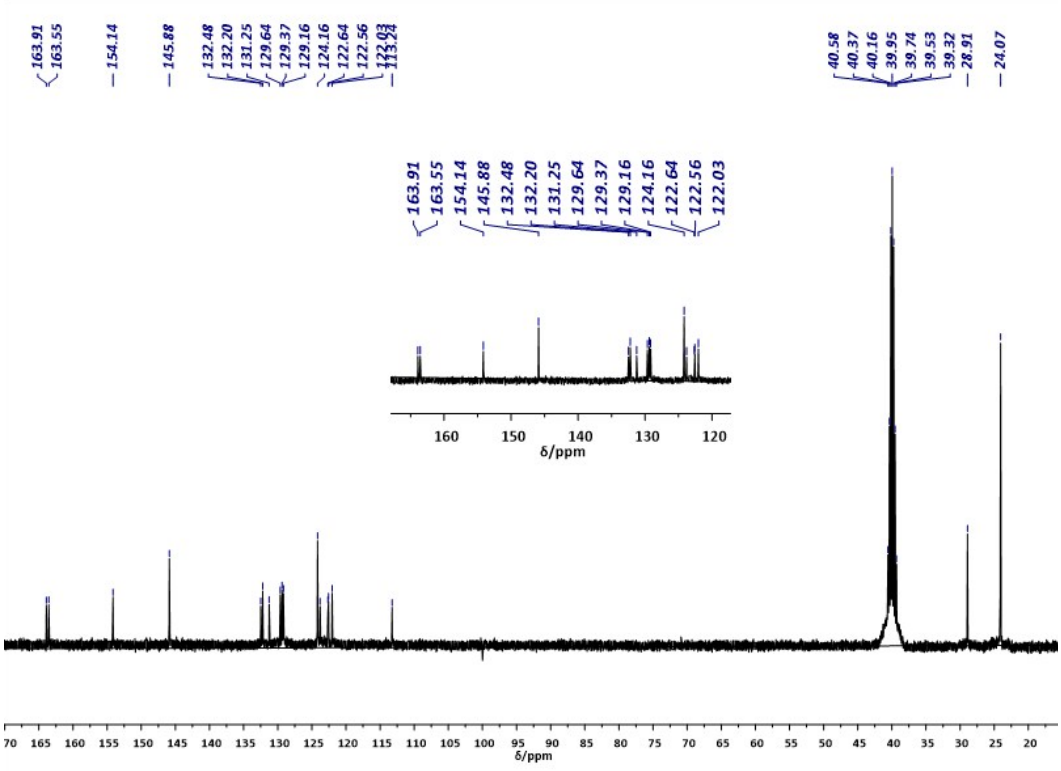

Figure S4. ^{13}C NMR spectrum of **3b** (100 MHz, d_6-DMSO, 298K)

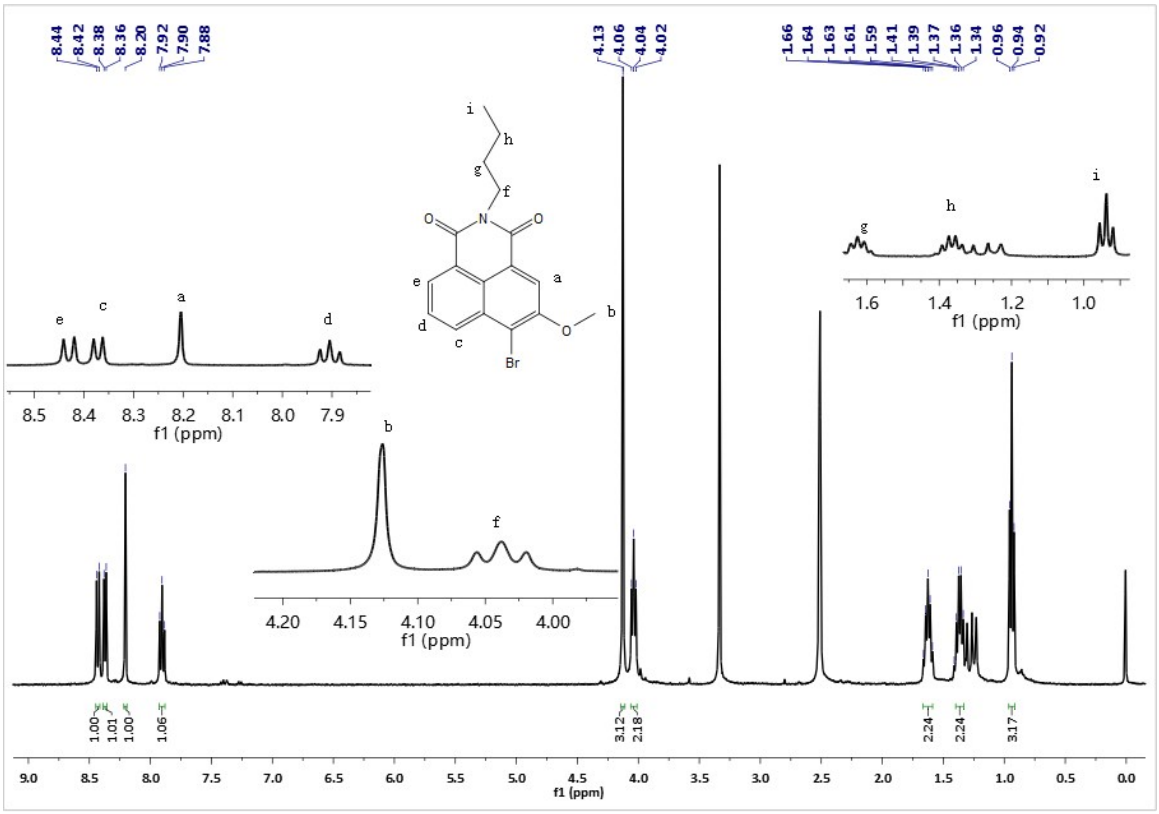

Figure S5. ^{1}H NMR spectrum of **4a** (400 MHz, d_6-DMSO, 298K)

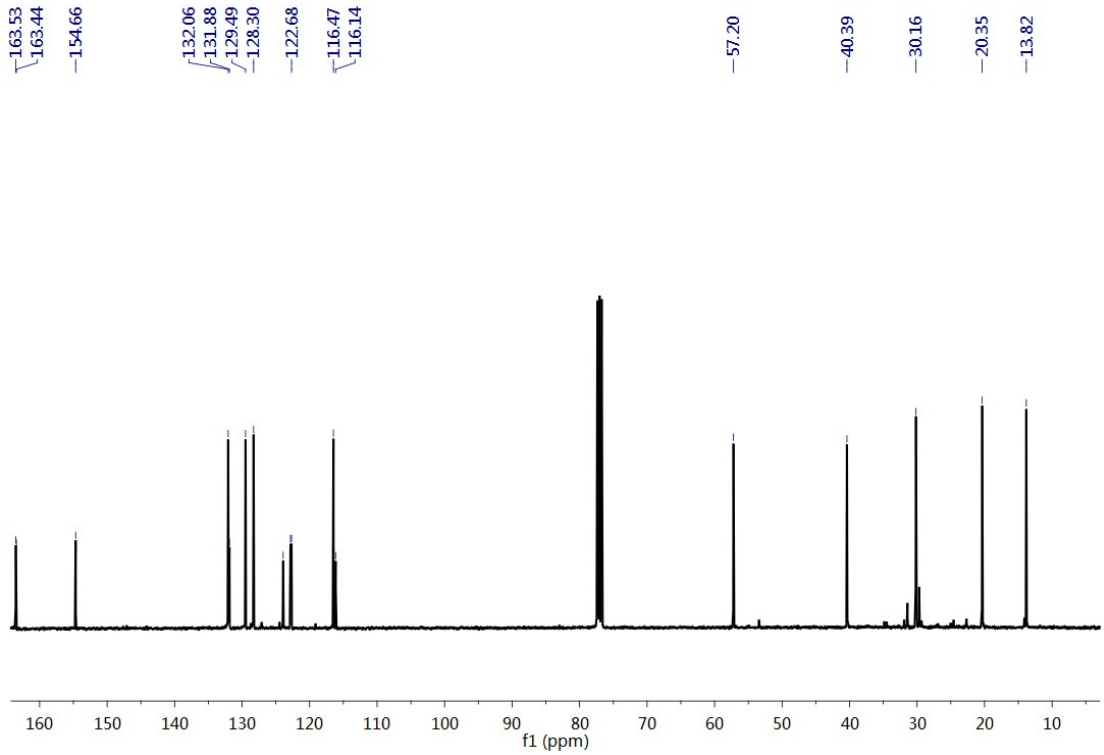

Figure S6. ^{13}C NMR spectrum of **4a** (100 MHz, $CDCl_3$, 298K)

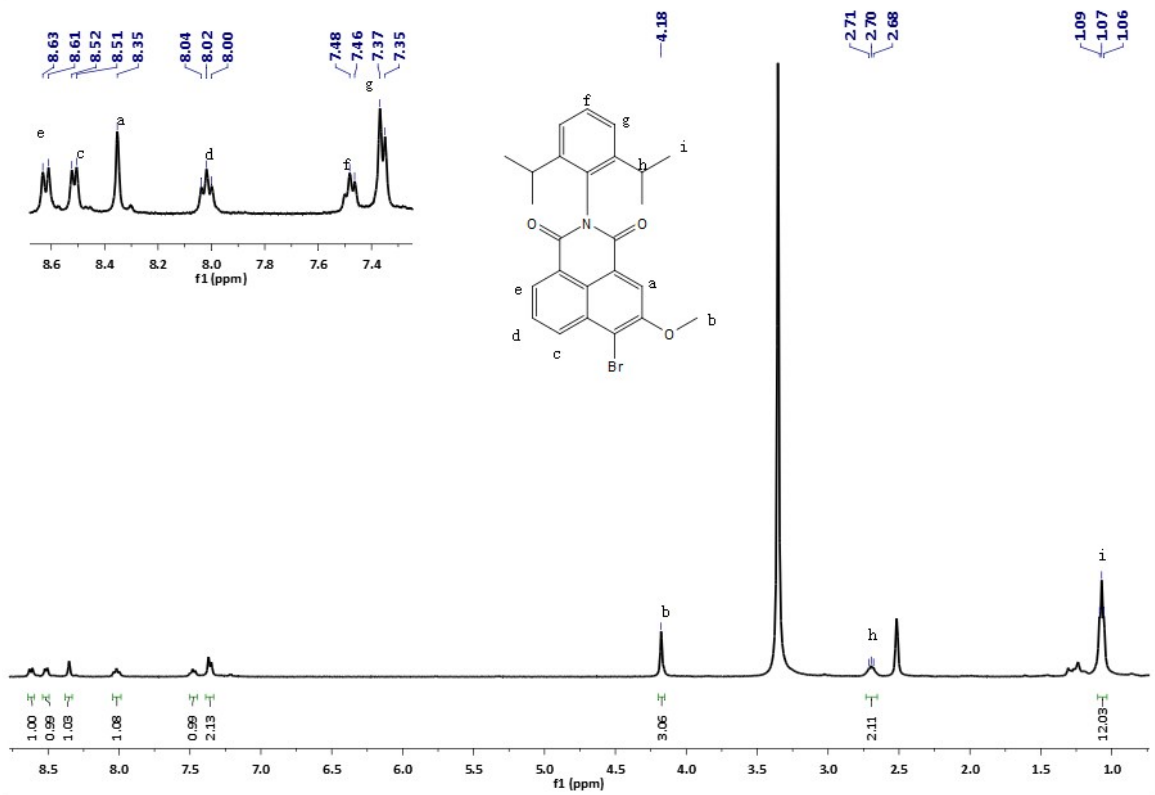

Figure S7. ^{1}H NMR spectrum of **4b** (400 MHz, d_6-DMSO, 298K)

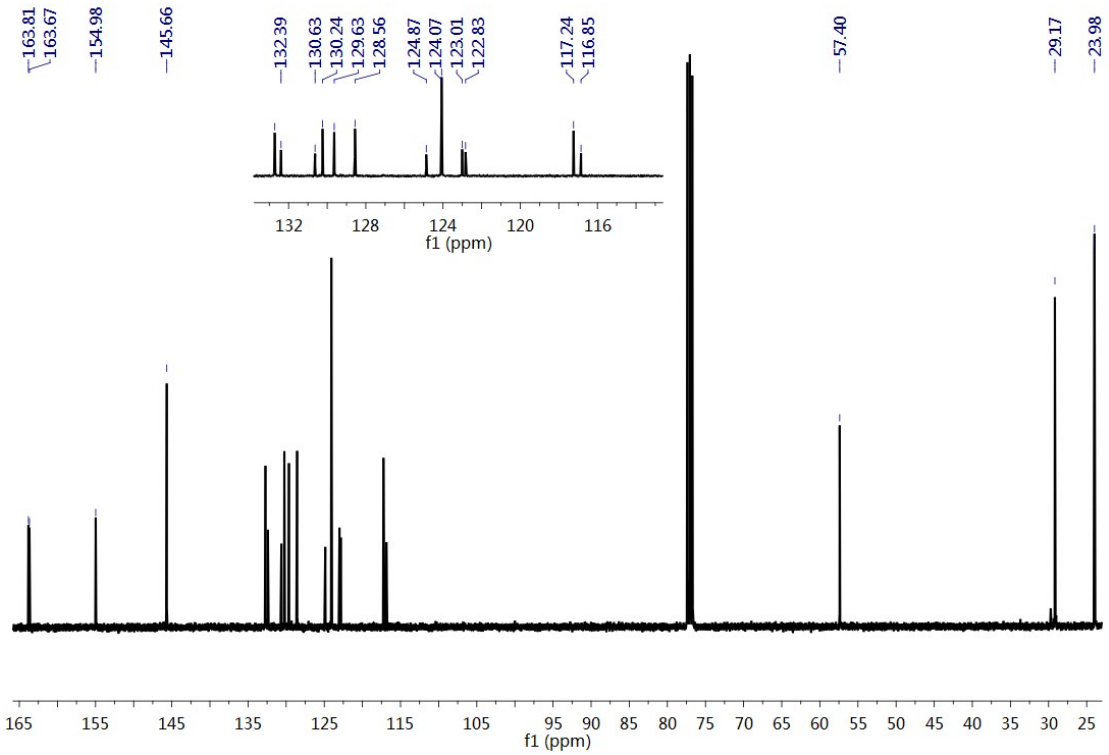

Figure S8. ^{13}C NMR spectrum of **4b** (100 MHz, $CDCl_3$, 298K)

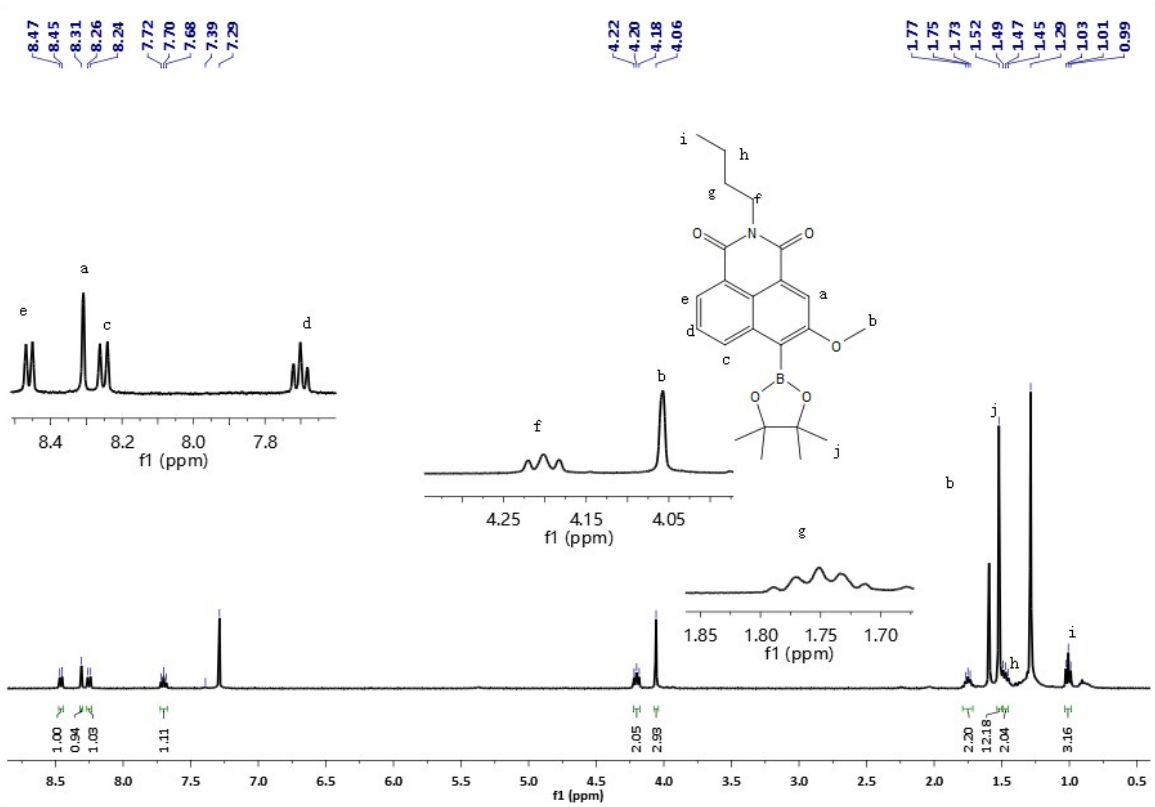

Figure S9. ^{1}H NMR spectrum of **5a** (400 MHz, $CDCl_3$, 298K)

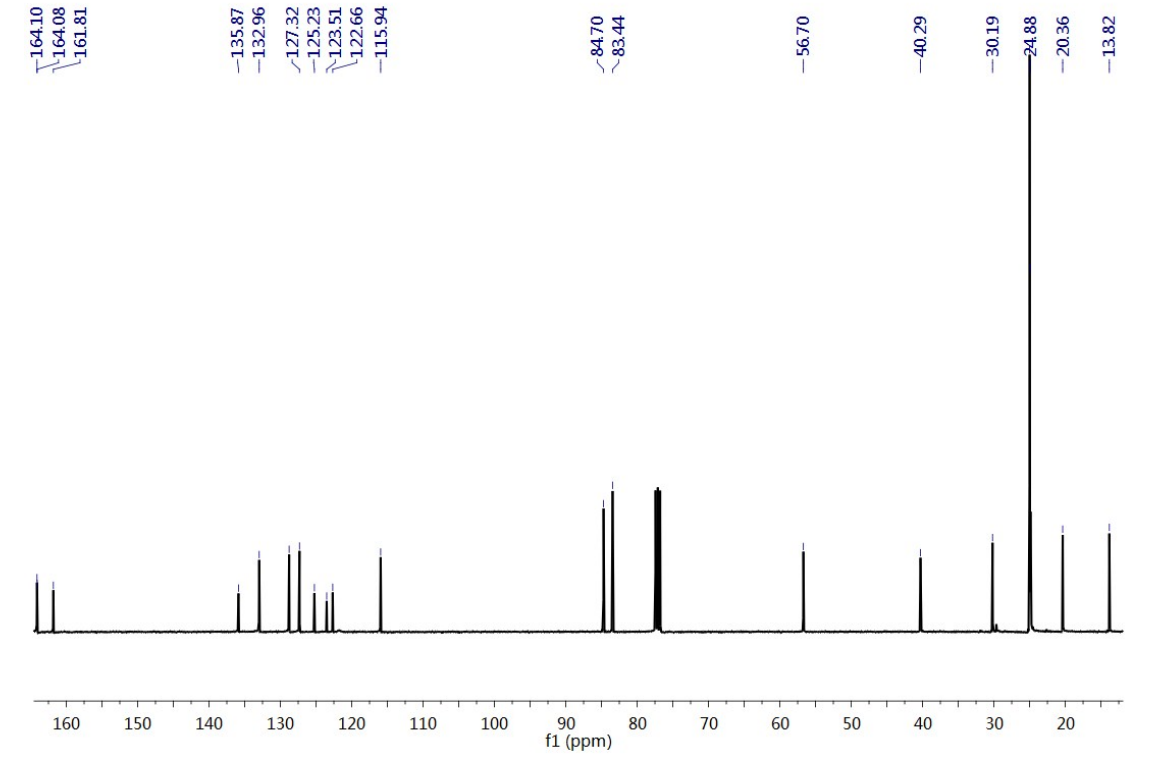

Figure S10. ^{13}C NMR spectrum of **5a** (100 MHz, $CDCl_3$, 298K)

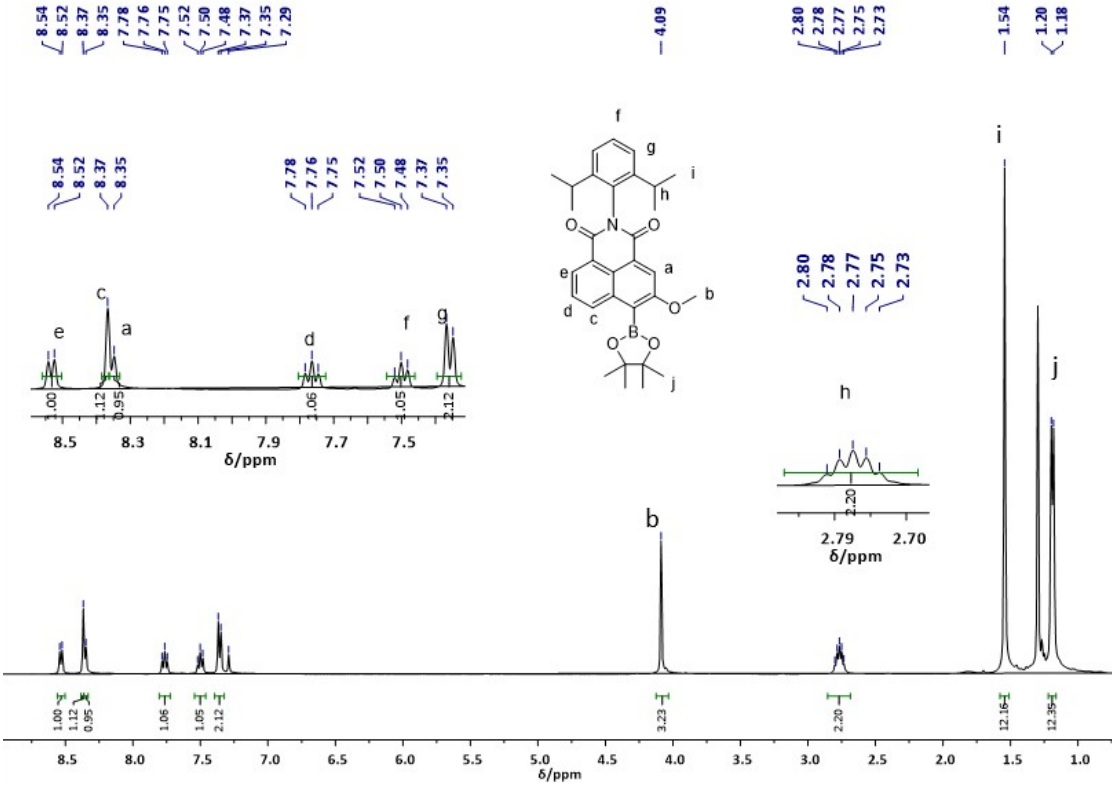

Figure S11. ^{1}H NMR spectrum of **5b** (400 MHz, d_6-Acetone, 298K)

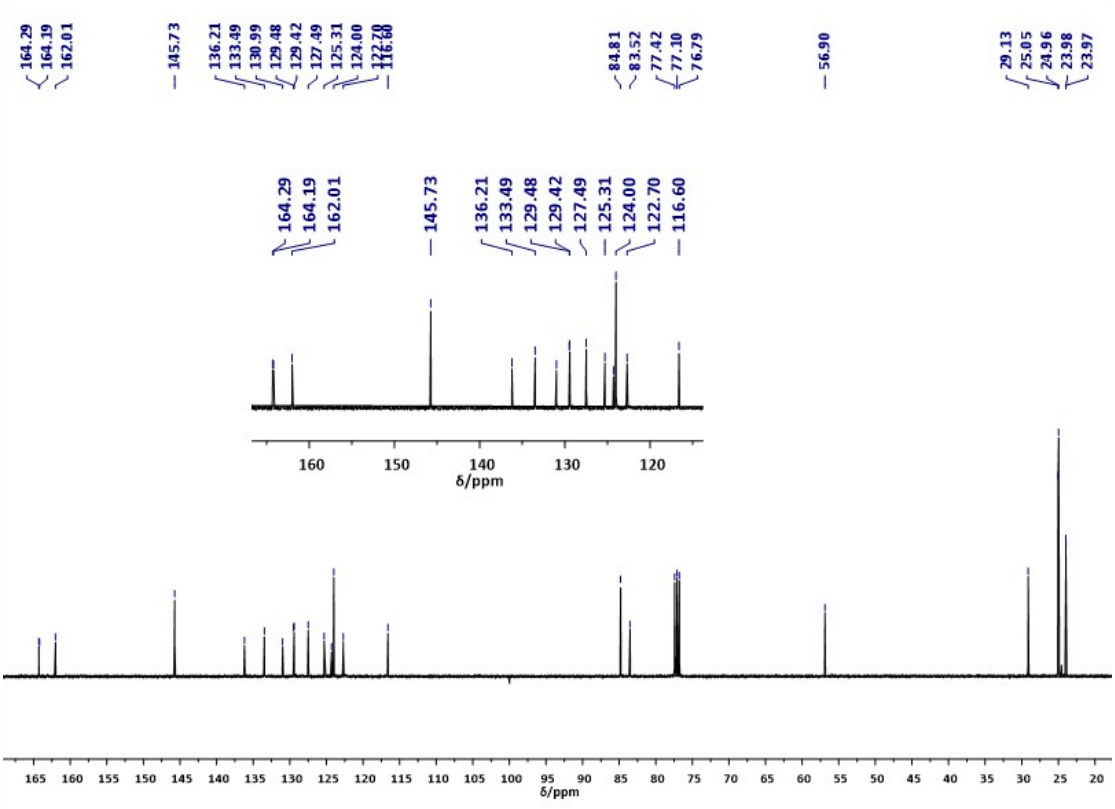

Figure S12. ^{13}C NMR spectrum of **5b** (100 MHz, $CDCl_3$, 298K)

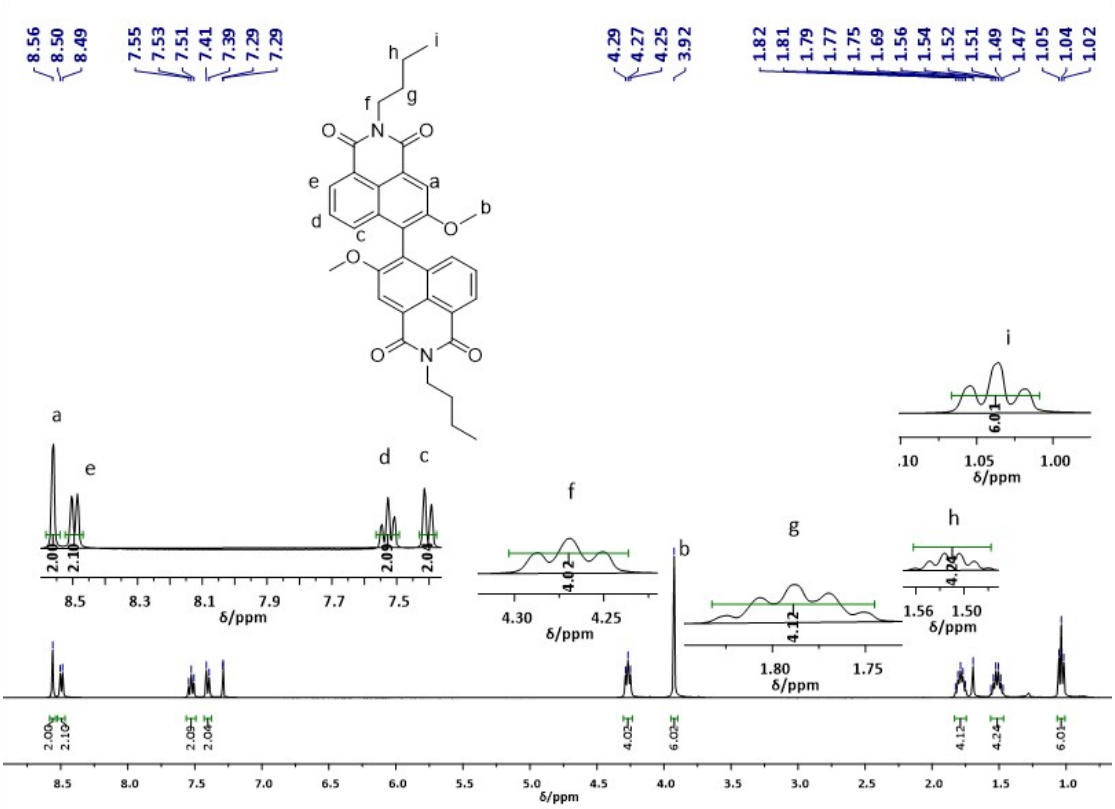

Figure S13. ^{1}H NMR spectrum of **6a** (400 MHz, $CDCl_3$, 298K)

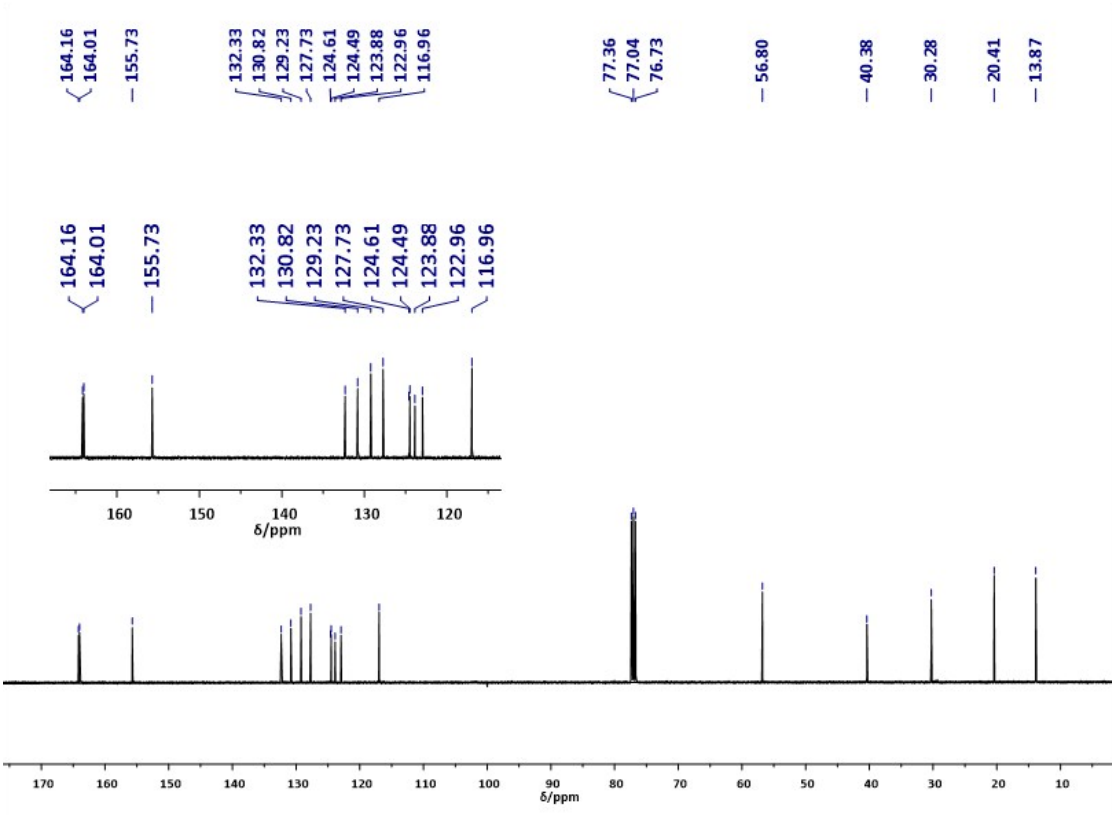

Figure S14. ^{13}C NMR spectrum of **6a** (100 MHz, $CDCl_3$, 298K)

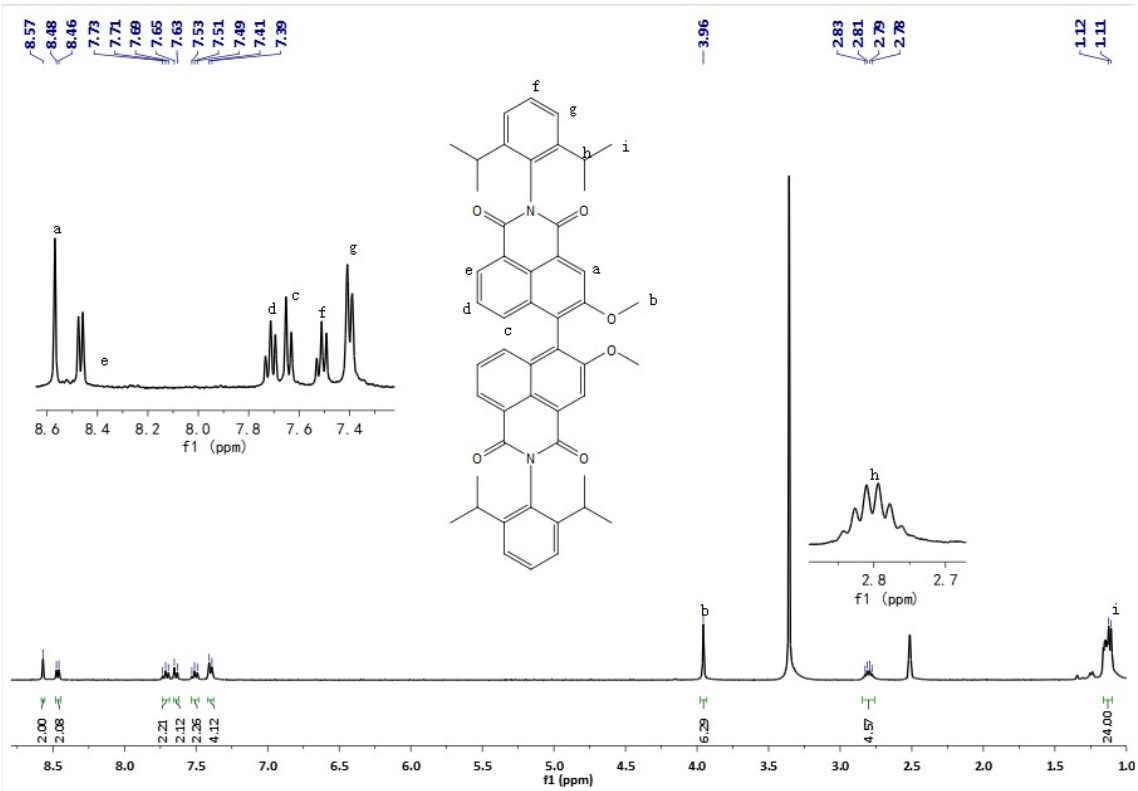

Figure S15. ^{1}H NMR spectrum of **6b** (400 MHz, d_6-DMSO, 298K)

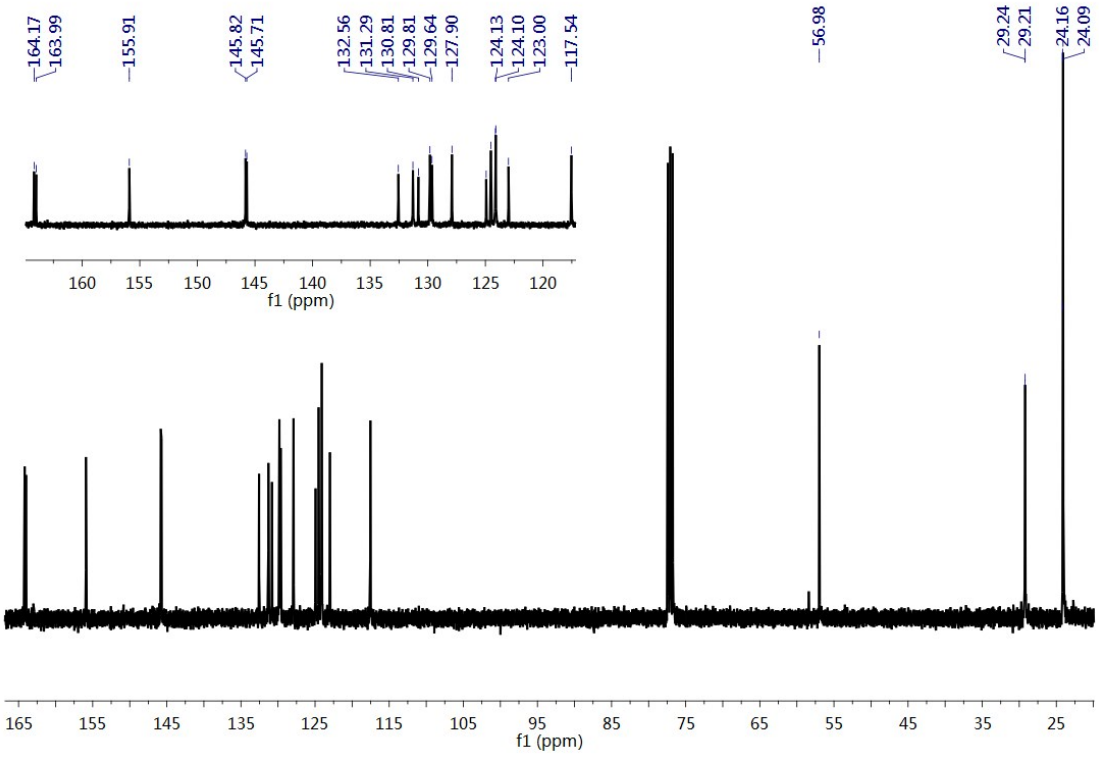

Figure S16. ^{13}C NMR spectrum of **6b** (100 MHz, $CDCl_3$, 298K)

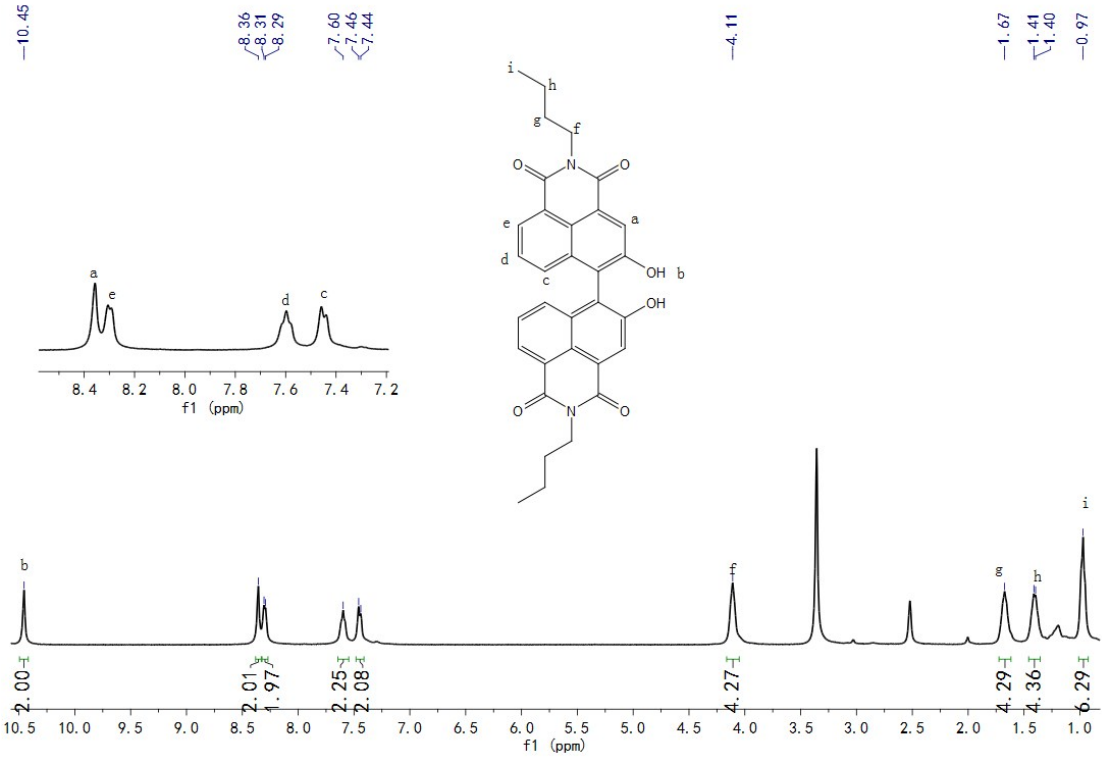

Figure S17. ^{1}H NMR spectrum of **1a** (400 MHz, d_6-DMSO, 298K)

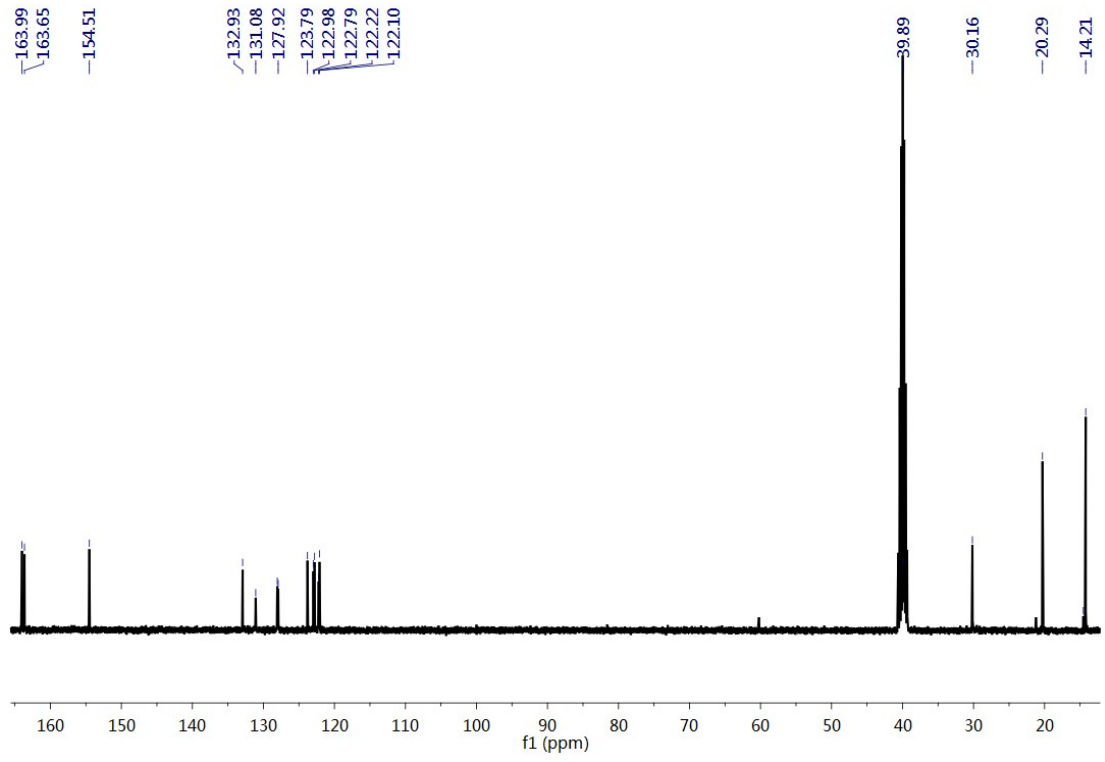

Figure S18. ^{13}C NMR spectrum of **1a** (100 MHz, d_6-DMSO, 298K)

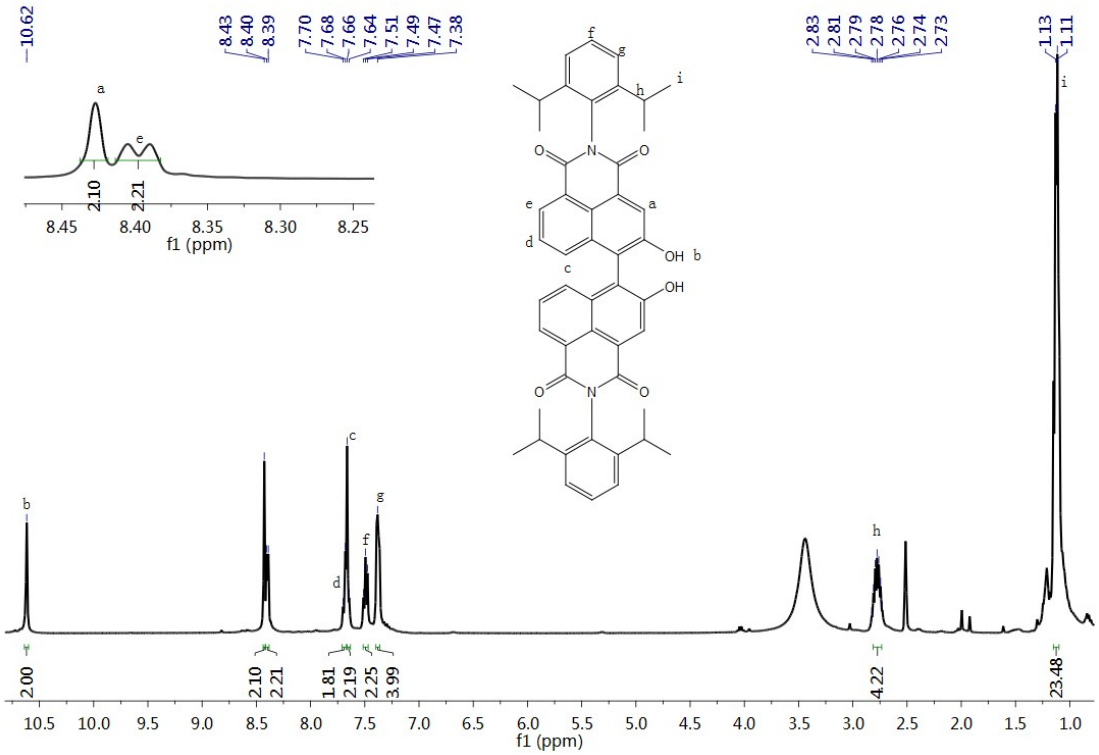

Figure S19. ^{1}H NMR spectrum of **1b** (400 MHz, d_6-DMSO, 298K)

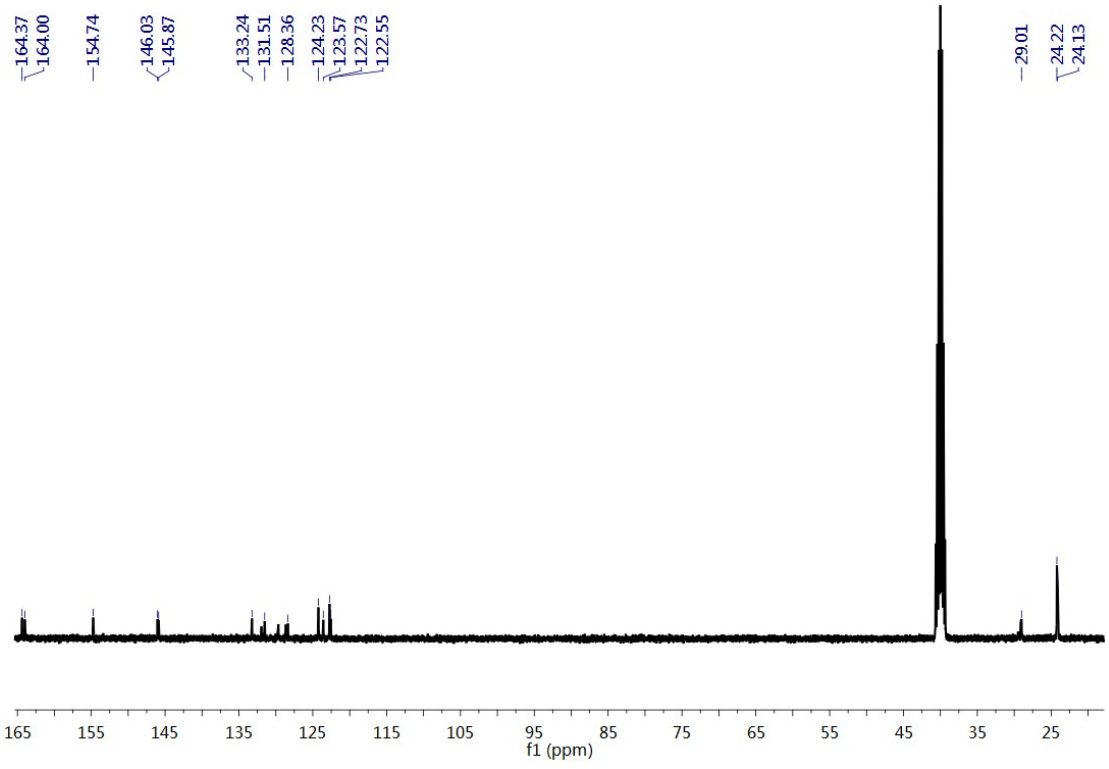

Figure S20. ^{13}C NMR spectrum of **1b** (100 MHz, d_6-DMSO, 298K)

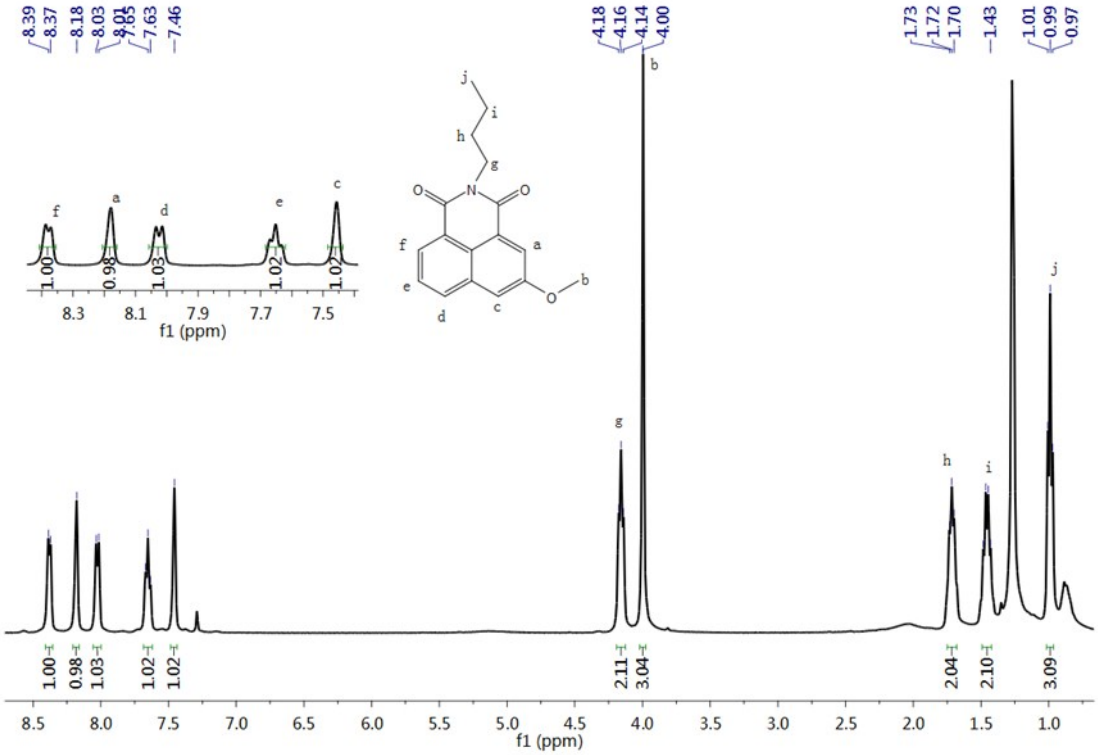

Figure S21. ^{1}H NMR spectrum of **7a** (400 MHz, $CDCl_3$, 298K)

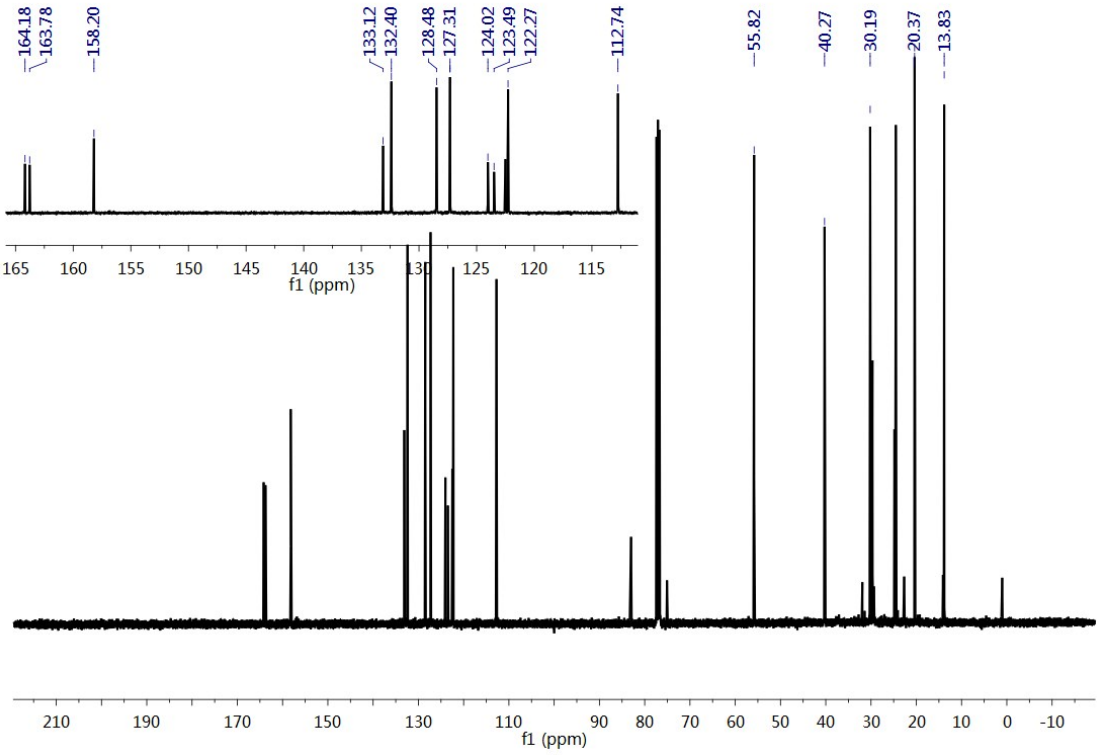

Figure S22. ^{13}C NMR spectrum of **7a** (100 MHz, $CDCl_3$, 298K)

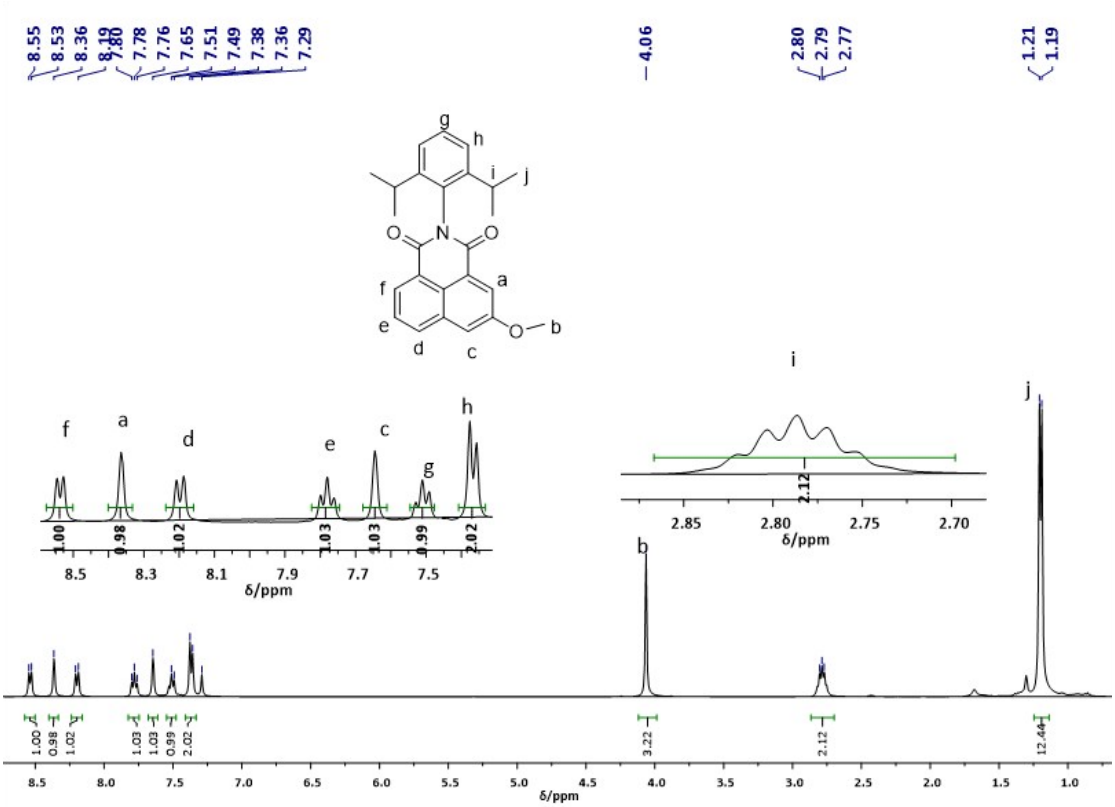

Figure S23. ^{1}H NMR spectrum of **7b** (400 MHz, $CDCl_3$, 298K)

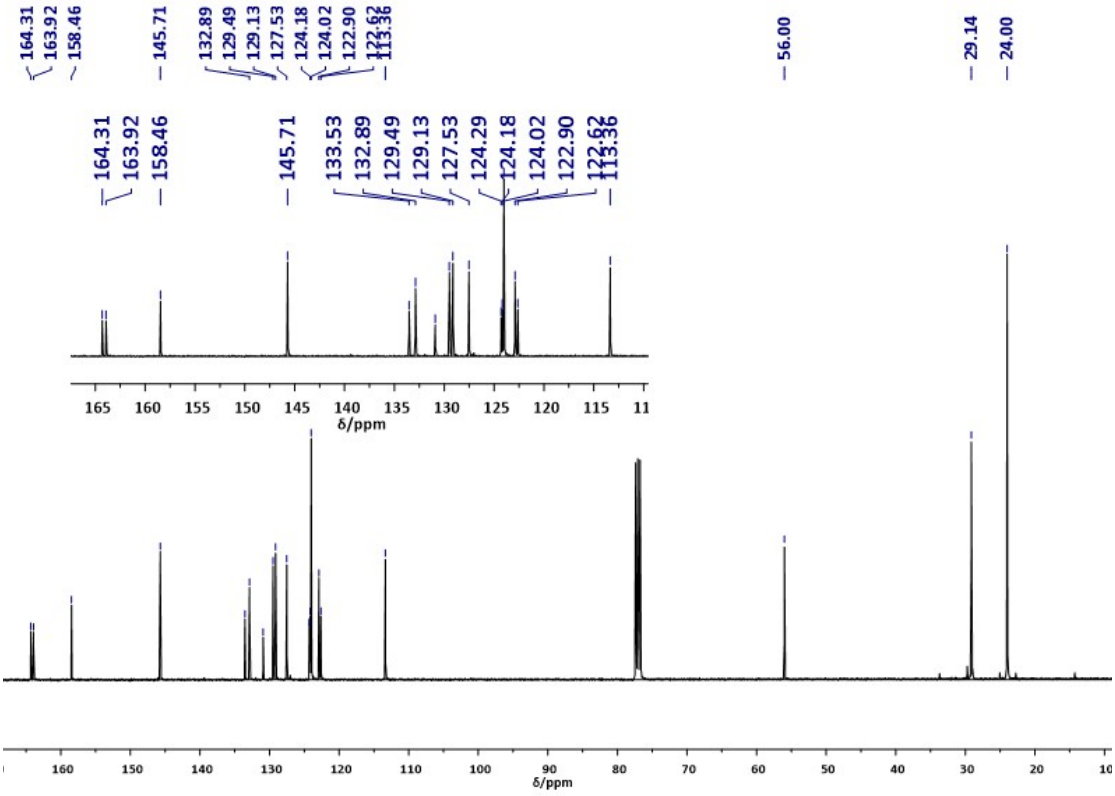

Figure S24. ^{13}C NMR spectrum of **7b** (100 MHz, $CDCl_3$, 298K)

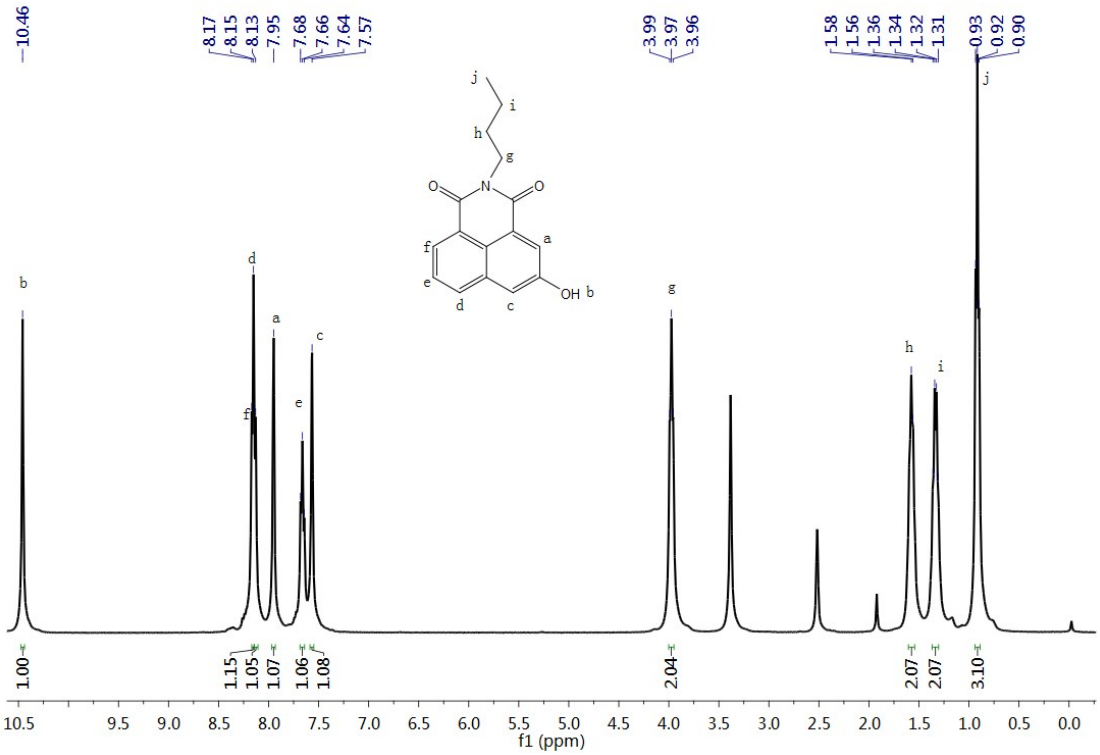

Figure S25. ^{1}H NMR spectrum of **8a** (400 MHz, d_6-DMSO, 298K)

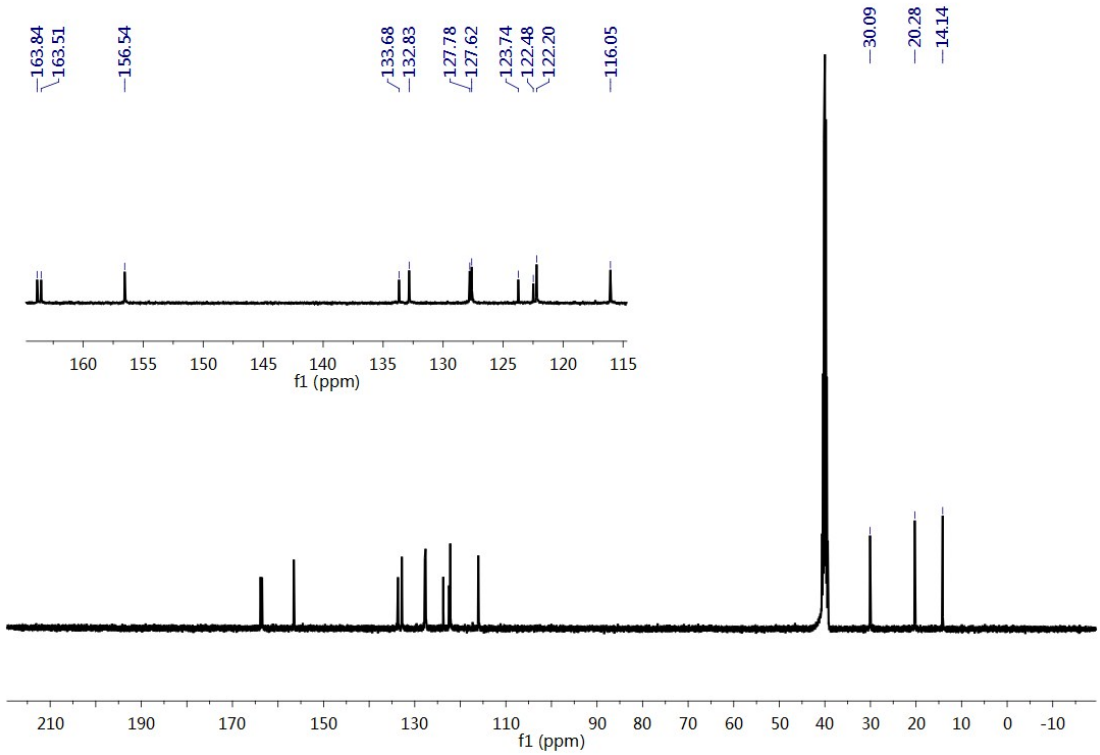

Figure S26. ^{13}C NMR spectrum of **8a** (100 MHz, d_6-DMSO, 298K)

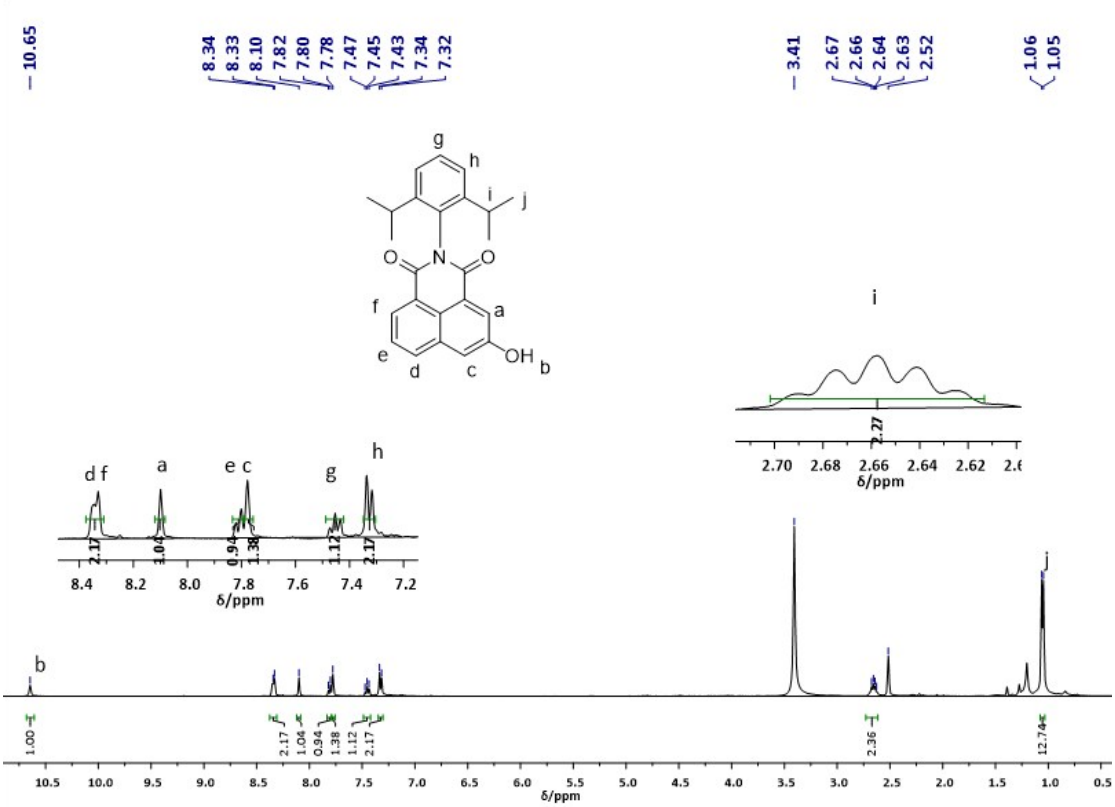

Figure S27. ^{1}H NMR spectrum of **8b** (400 MHz, d_6-DMSO, 298K)

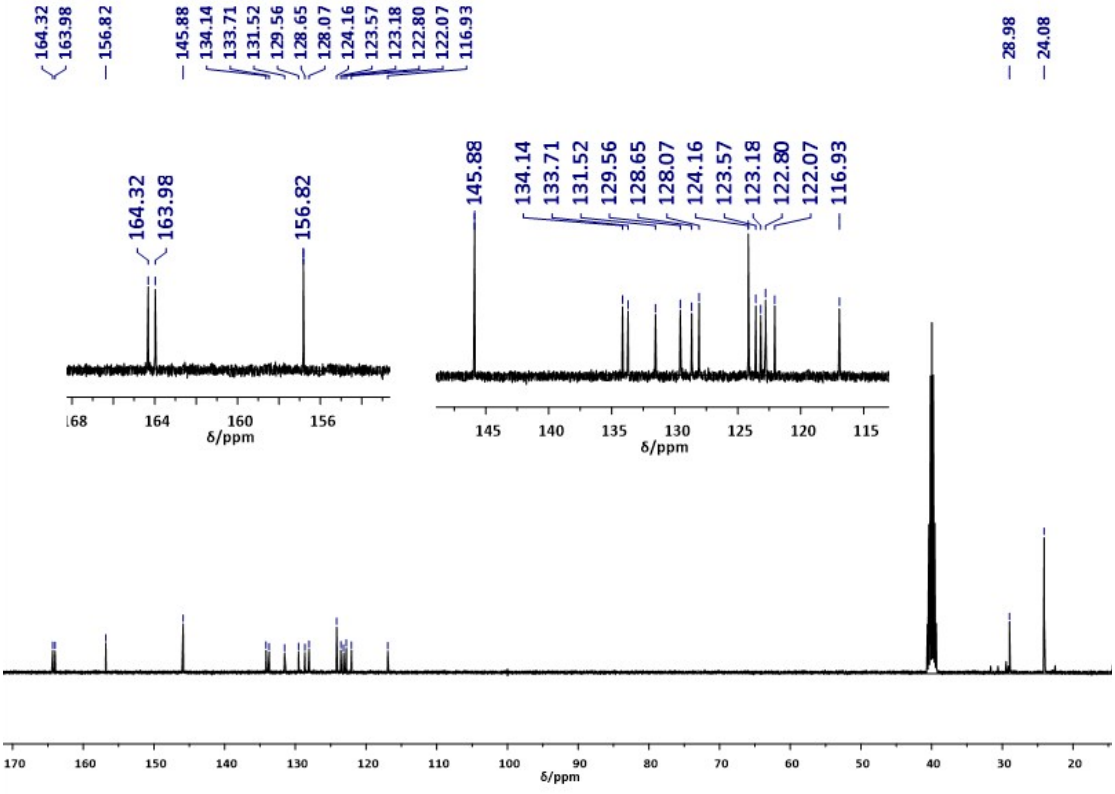

Figure S28. ^{13}C NMR spectrum of **8b** (100 MHz, d_6-DMSO, 298K)

2. High-resolution mass spectra (HRMS)

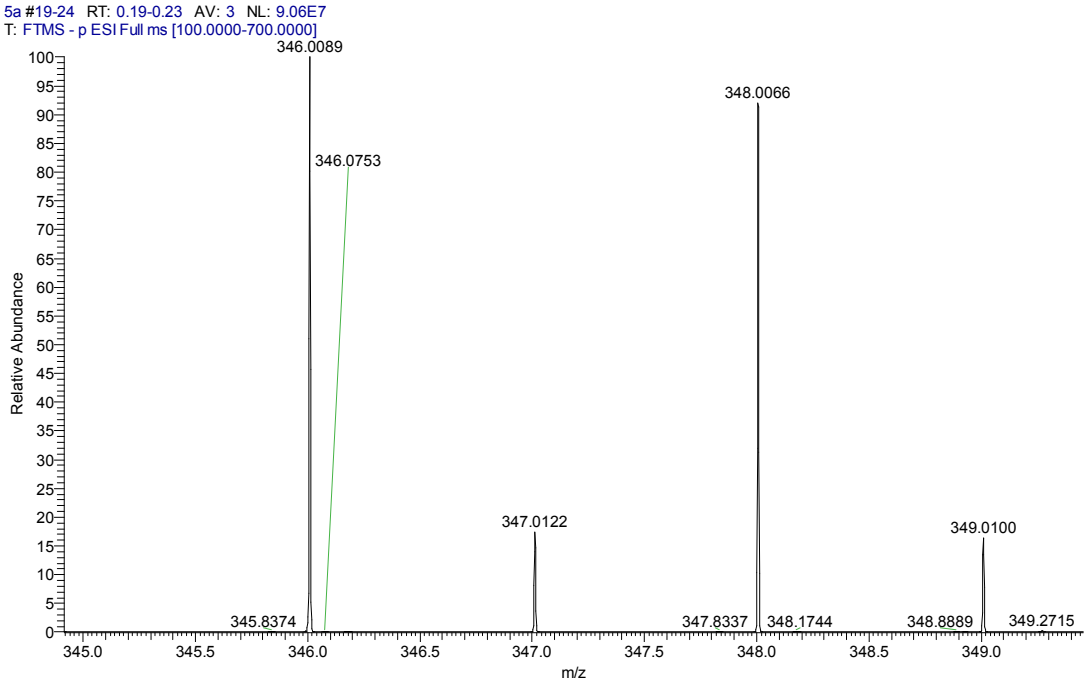

Figure S29. ESI mass spectrum of **3a** in DMSO in negative mode

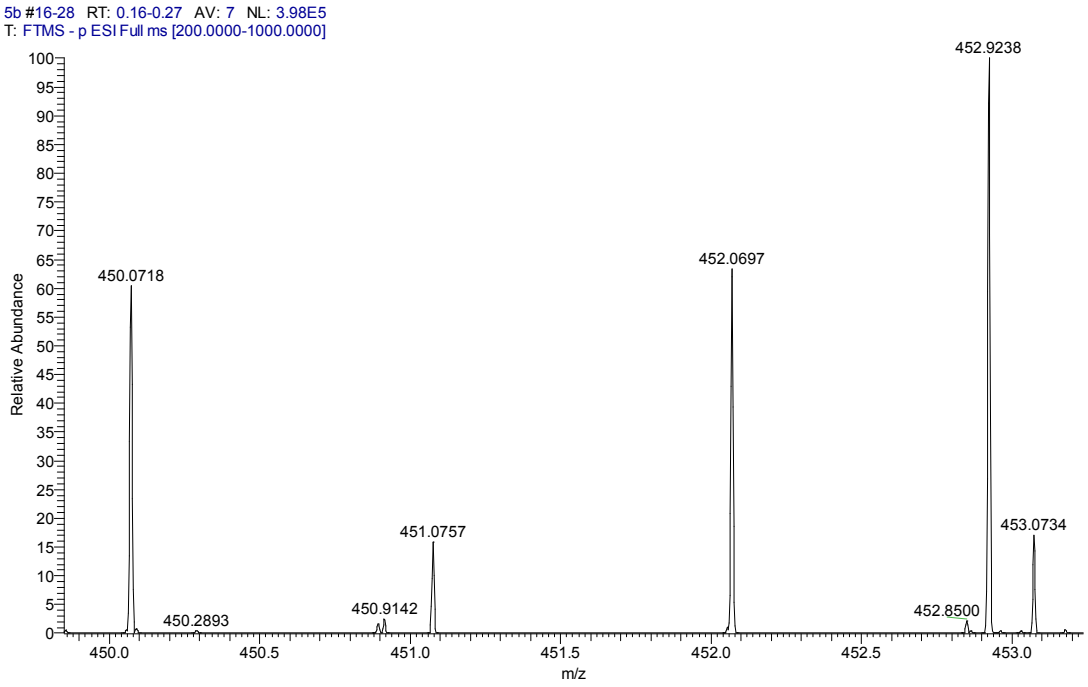

Figure S30. ESI mass spectrum of **3b** in DMSO in negative mode

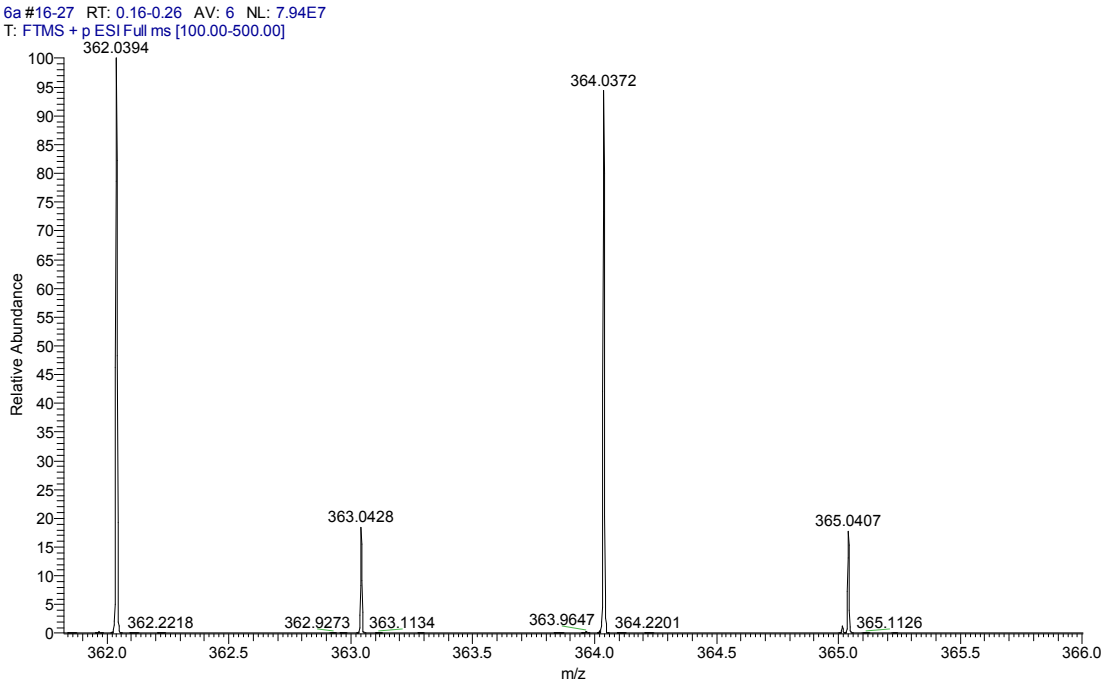

Figure S31. ESI mass spectrum of **4a** in DCM in positive mode

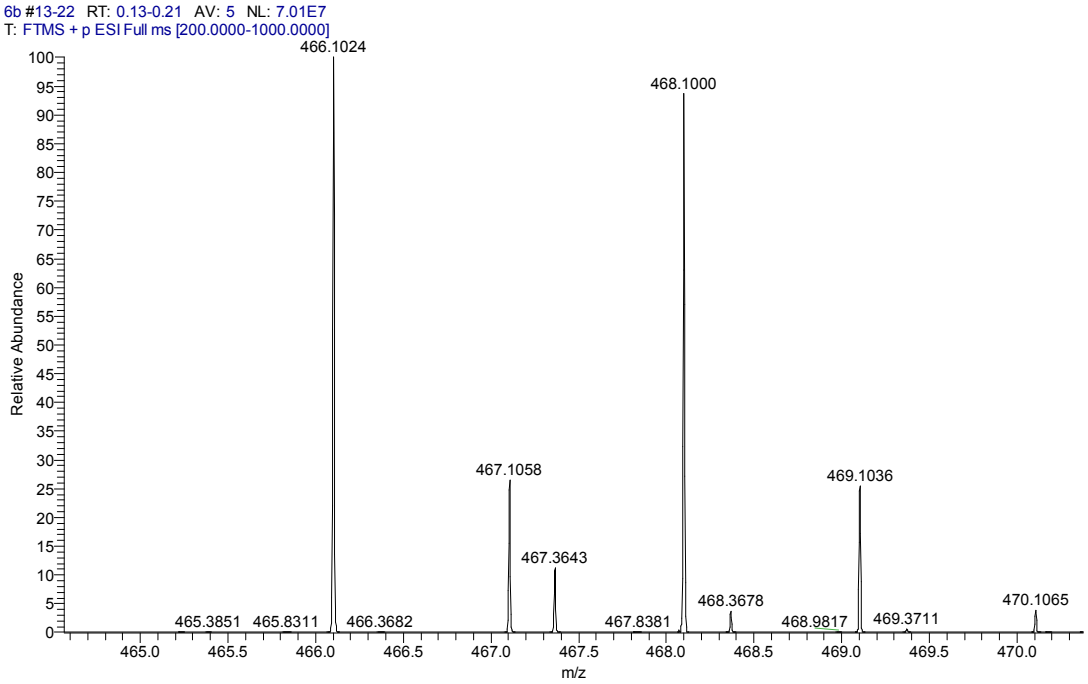

Figure S32. ESI mass spectrum of **4b** in DCM in positive mode

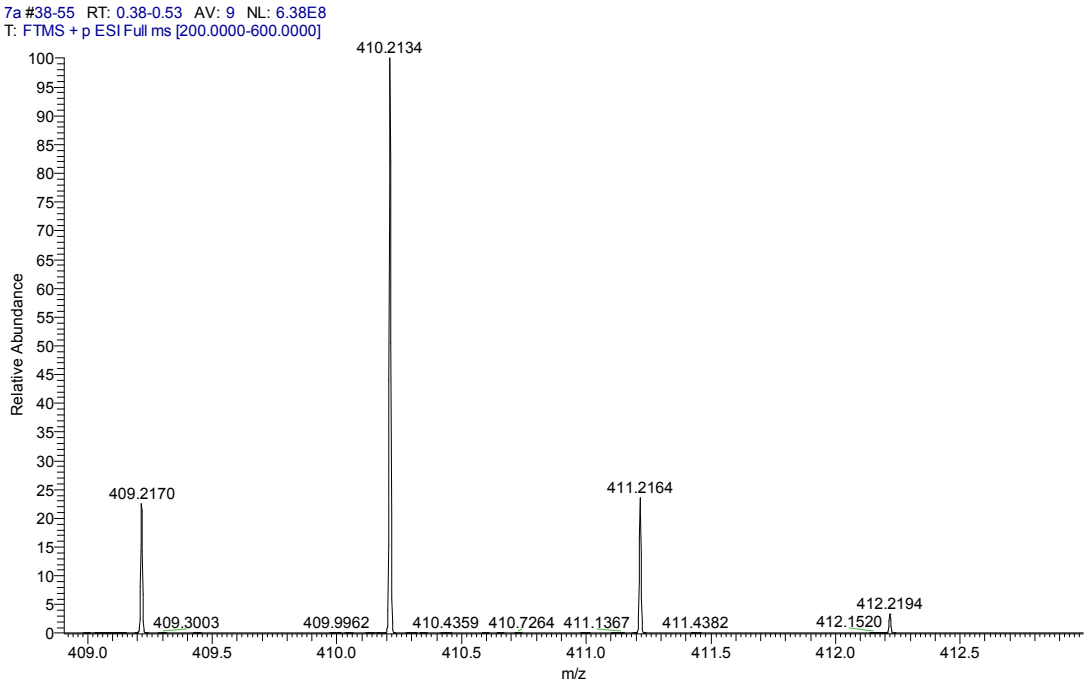

Figure S33. ESI mass spectrum of **5a** in DCM in positive mode

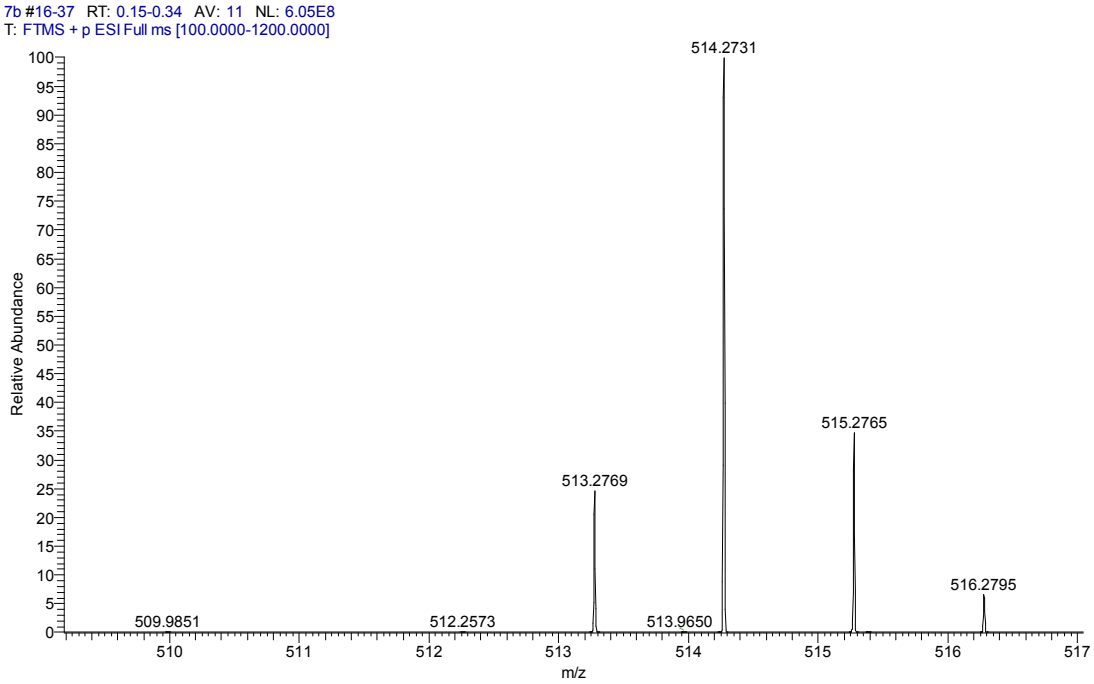

Figure S34. ESI mass spectrum of **5b** in DCM in positive mode

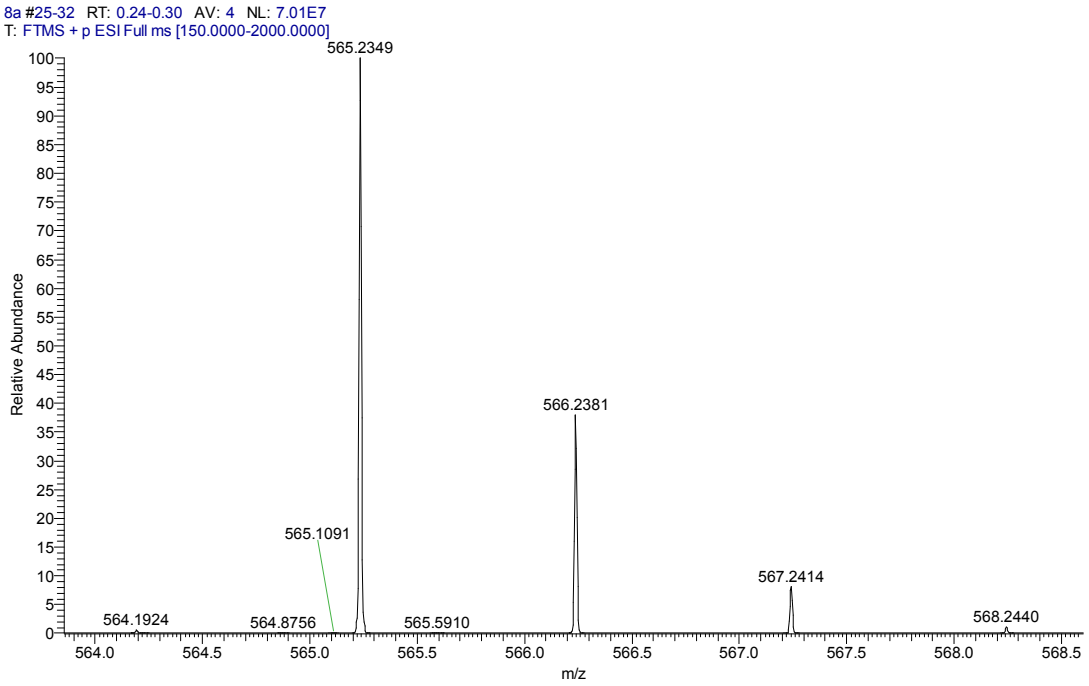

Figure S35. ESI mass spectrum of **6a** in DCM in positive mode

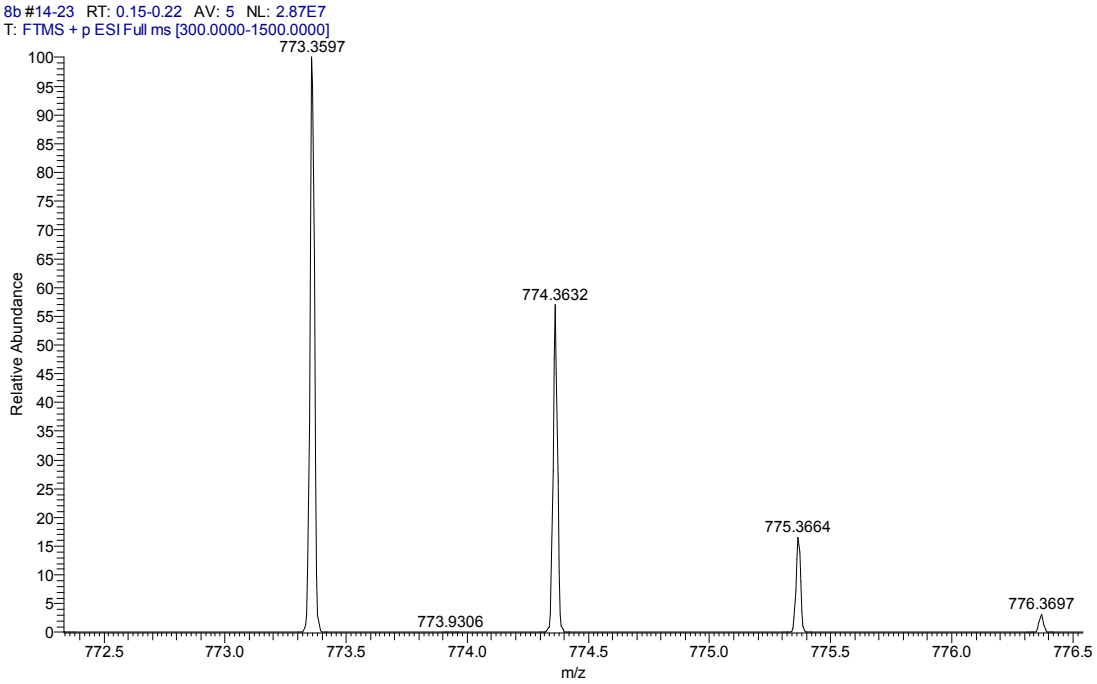

Figure S36. ESI mass spectrum of **6b** in DCM in positive mode

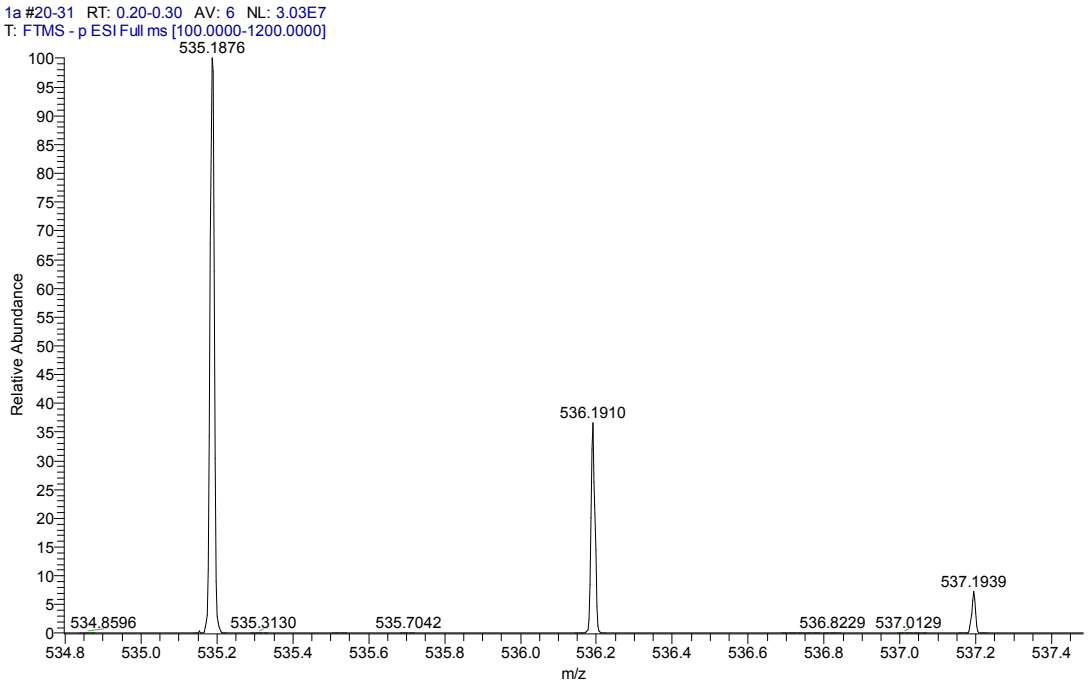

Figure S37. ESI mass spectrum of **1a** in DMSO in negative mode

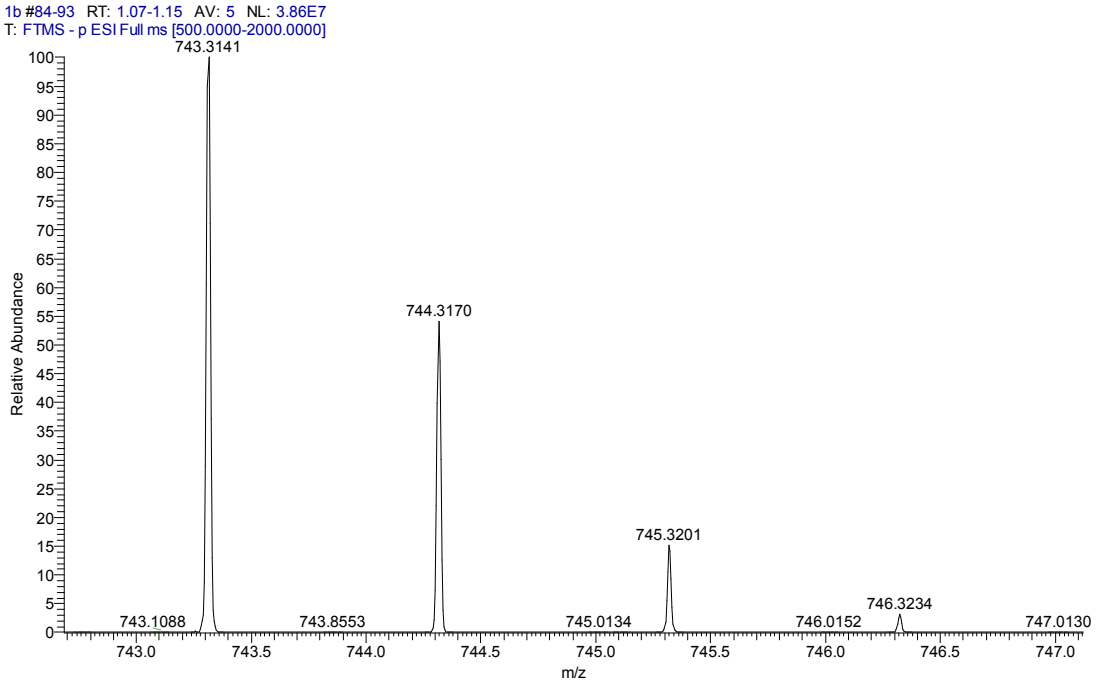

Figure S38. ESI mass spectrum of **1b** in DMSO in negative mode

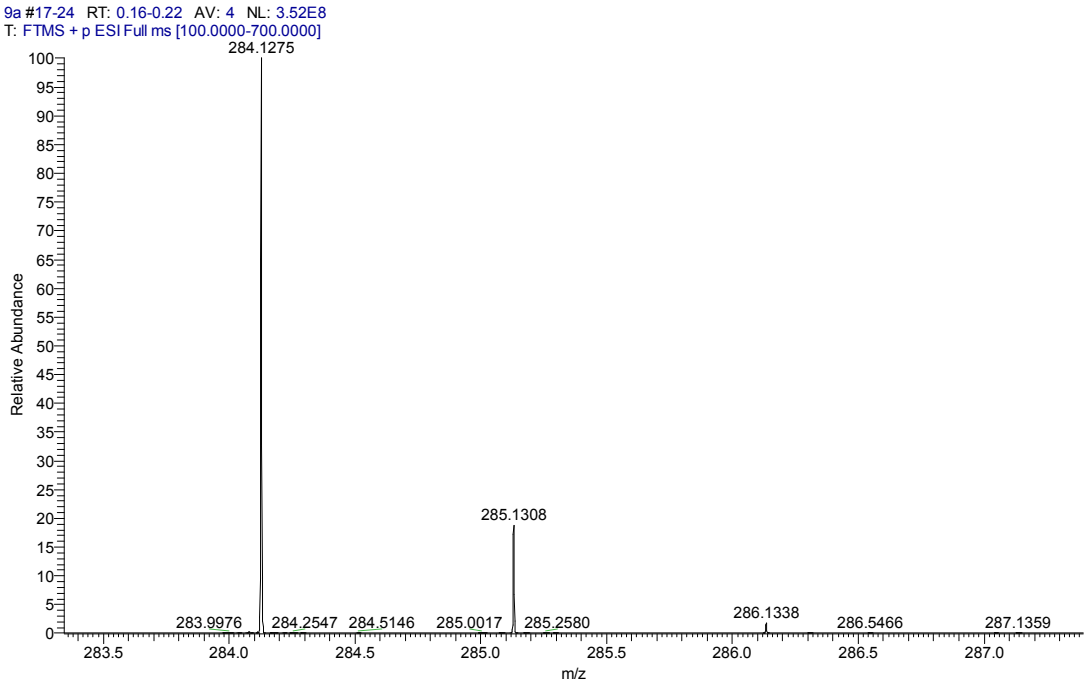

Figure S39. ESI mass spectrum of **7a** in DCM in positive mode

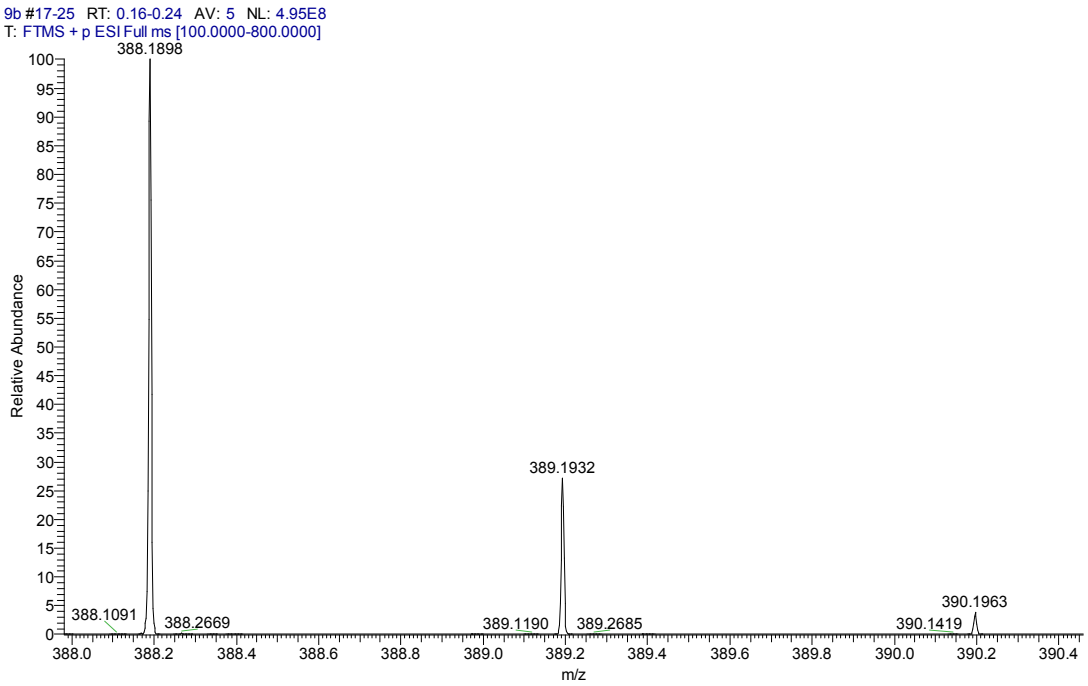

Figure S40. ESI mass spectrum of **7b** in DCM in positive mode

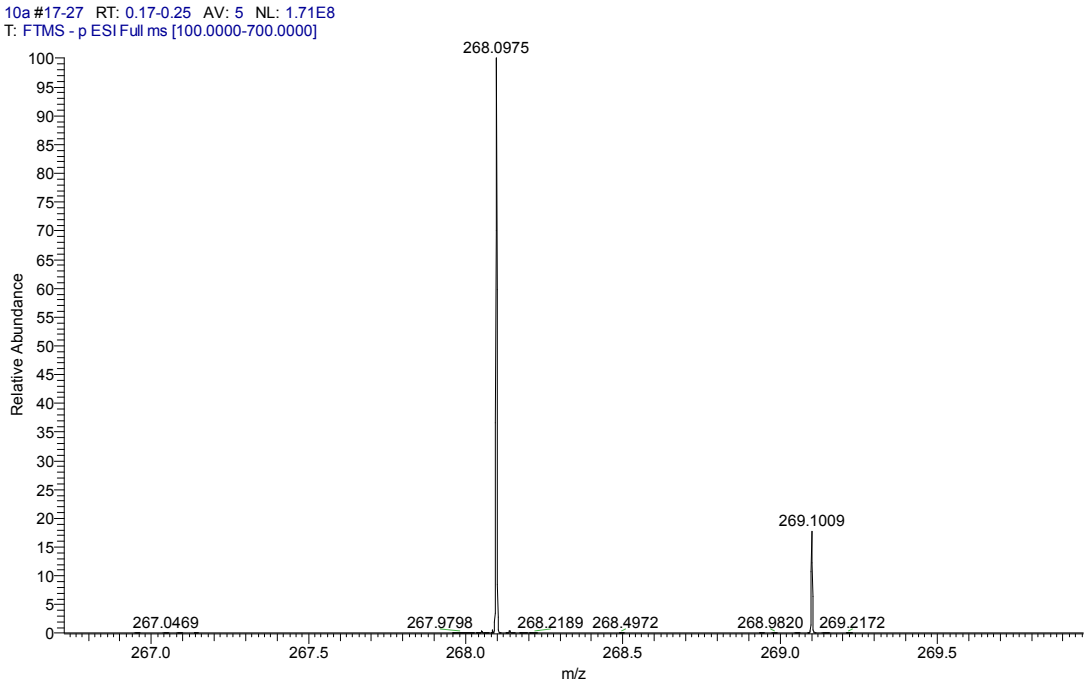

Figure S41. ESI mass spectrum of **8a** in DMSO in negative mode

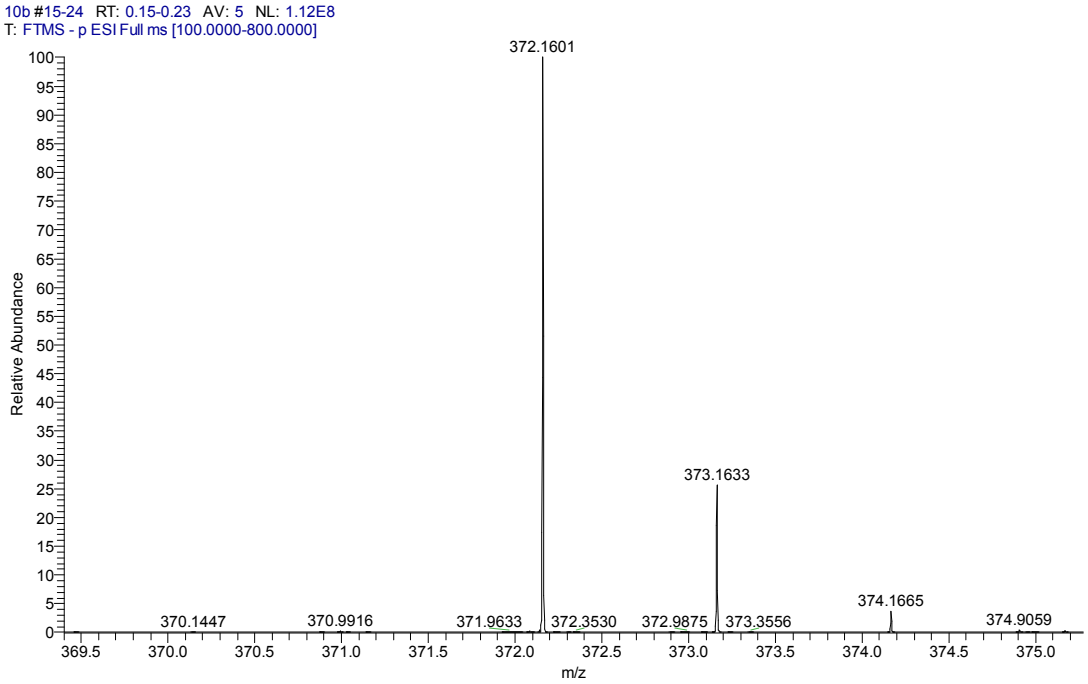

Figure S42. ESI mass spectrum of **8b** in DMSO in negative mode

3. Single-crystal X-ray diffraction analyses

3.1 *Methods and crystal data*

Single crystals of **2** and **3** suitable for X-ray diffraction analyses were obtained by evaporation of their water and dimethyl sulfoxide solutions, respectively, while those of **4b**, **6a**, **6b** and **1a** were obtained by dissolving each of them in a solvent mixture (dichloromethane/ethanol = 90:10), followed by slow evaporation of the solvents within several days. However, single crystals of **2**, **3a**, **3b**, **4a**, **5a**, **5b** and **1b** obtained were too small to for the measurements in spite of several attempts by changing the solvents and methods.

Crystal data for **4b**, **6a**, **6b** and **1a** were collected using a Rigaku-AFC7 equipped with a Rigaku Saturn CCD area-detector system. The measurement was made by using graphic monochromatic Mo Kα radiation (λ = 0.71073 Å) under a cold nitrogen stream. The frame data were integrated and absorption correction using a Rigaku Crystal Clear program package. All calculations were performed with the *SHELXTL-97* program package, [S1-S3] and structures were solved by direct methods and refined by full-matrix least-squares against F^2. All non-hydrogen atoms were refined anisotropically, and hydrogen atoms of the organic ligands were generated theoretically onto the specific atoms. Crystallographic data are summarized as followings and have been deposited in the Cambridge Crystallographic Data Center as supplementary publication number CCDC 1856478, 1854207, 1854208 , 1894292 for **4b**, **6a**, **6b** and **1a**, respectively, which can be obtained free of charge from the Cambridge Crystallographic Data Center via www.ccdc.cam.ac.uk/data_request/cif.

Crystal data for **4b**: empirical formula $C_{25}H_{24}NO_3Br$, formula weight 465.09, T = 293(2) K, wavelength 0.71073 Å, crystal system: monoclinic, space group $P2_1/n$, unit cell dimensions a = 12.2045(9) Å, b = 12.4239(7) Å, c = 14.9788(12) Å, α = 90°, β = 100.238°(8), γ = 90°, V = 2235.0(3) $Å^3$, Z = 10, ρ_{cal} = 1.279 g / cm^3, absorption coefficient, 0.083mm^{-1}, F(000) = 910.0, crystal size 0.55 × 0.45 × 0.40 mm^3, theta range for data collection 7.119° to 58.604°, index ranges -16<=h<=15; -16<=k<=15; -19<=l<=20, reflections collected 19756, independent reflections, 5148 [R (int) = 0.0656,R(sigma) = 0.1003], GooF(F^2) = 1.024, R_1 = 0.0664, wR_2 = 0.1261 for I >= 2sigma (I), R_1 = 0.1598,wR_2 = 0.1497 for all data, data completeness 0.842 and largest diff. peak and hole, 0.85 and -0.70 e. $Å^{-3}$.

Crystal data for **6a**: empirical formula $C_{34}H_{32}N_2O_6$, formula weight 564.23, T = 293(2) K, wavelength 0.71073 Å, crystal system: triclinic, space group P-1, unit cell dimensions a = 10.4723(7) Å, b = 12.7127(9) Å, c = 12.7391(9) Å, α = 113.157°(7), β = 97.019°(6), γ = 110.996°(6), V =1385.74(19) $Å^3$, Z =2, ρ_{cal} = 1.343 g / cm^3, absorption coefficient, 0.093 mm^{-1}, F(000) = 587.0, crystal size 0.26 × 0.16 × 0.10 mm^3, theta range for data collection 3.654° to 59.584°, index ranges -13<=h<=12; -15<=k<=16; -15<=l<=17, reflections collected 20408, independent reflections, 6490 R (int) = 0.0401, R(sigma) = 0.0491], GooF(F^2) = 1.071, R_1 = 0.0784, wR_2 = 0.2369 for I >= 2sigma (I), R_1 = 0.1197,wR_2 = 0.2764 for all data, data completeness 0.817 and largest diff. peak and hole, 1.02 and -0.42 e. $Å^{-3}$.

Crystal data for **6b**: empirical formula $C_{50}H_{48}N_2O_6$, formula weight 772.35, T = 293(2) K, wavelength 0.71073 Å, crystal system: triclinic, space group P-1, unit cell dimensions a = 12.2870(13) Å, b = 13.2979(16) Å, c = 27.850(4) Å, α = 86.660°(13), β = 90°, γ = 10°, V =4542.7(10) $Å^3$, Z =2, ρ_{cal} = 1.177 g / cm^3, absorption coefficient, 0.078mm^{-1}, F(000) = 1712.0, crystal size 0.30 × 0.25 × 0.14 mm^3, theta range for data collection 7.056°to 46.512°, index ranges -13<=h<=12; -14<=k<=14; -30<=l<=24, reflections collected 25172, independent reflections, 12376 [R (int) = 0.1058, R (sigma) = 0.2130], GooF(F^2) = 1.008, R_1 = 0.1070, wR_2 = 0.2667 for I >= 2sigma (I), R_1 = 0.2354,wR_2 = 0.3490 for all data, data completeness 0.949 and largest diff. peak and hole, 0.47 and -0.26 e. $Å^{-3}$.

Crystal data for **1a**: empirical formula $C_{32}H_{28}N_2O_6$, formula weight 536.23, T = 293(2) K, wavelength 1.54184 Å, crystal system: orthorhombic, space group Pna21, unit cell dimensions a = 32.9749(8) Å, b = 12.7486(2) Å, c = 24.5123(6) Å, α = 90°, β = 90°, γ = 90°, V =10298.3(4) $Å^3$, Z =4, ρ_{cal} = 1.361 g / cm^3, absorption coefficient, 0.779mm^{-1}, F(000) = 4418.0, crystal size 0.2 × 0.12 × 0.08 mm^3, theta range for data collection 3.2120° to 73.9060°, index ranges -41<=h<=41; -15<=k<=16; -25<=l<=31, reflections collected 20878, independent reflections, 11364 R (int) = 0.894, R(sigma) = 0.940], GooF(F^2) = 1.351, R_1 = 0.1779, wR_2 = 0.3425 for I >= 2sigma (I), R_1 = 0.1534,wR_2 = 0.3669 for all data, data completeness 0.940 and largest diff. peak and hole, 1.083 and -0.468 e. $Å^{-3}$.

3.2 *The molecular structure of 4b*

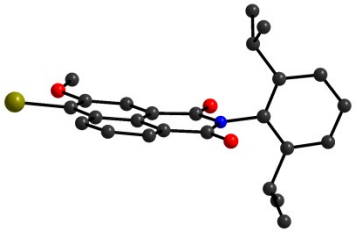

Figure S43. Molecular structure of **4b** in the single crystal the single crystal as determined by single crystal X-ray analysis at 293 K. Hydrogen atoms are omitted for clarity

4. Chiral HPLC analyses of 6a, 6b, 1a, 1b, (R)-1a

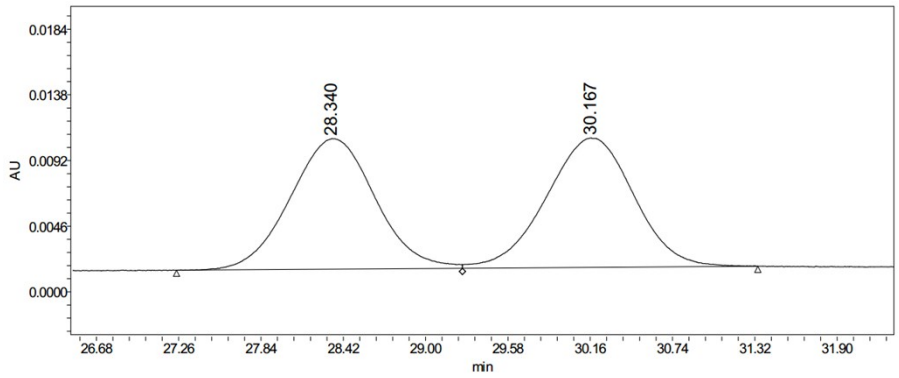

Figure S44. HPLC chromatogram of **6a** on a CHIRALPAK chiral- NR column (Φ = 0.46 cm) at ambient conditions using a mixture solution of cyclohexane and isopropanol (1:1 in volume) as eluent (flow rate 0.5 mL/min).

Table S1. The chiral HPLC chromatographic data of **6a** on a CHIRALPAK chiral-NR column (Φ = 0.46 cm) at ambient conditions

Peak	Processed channel	Ret. Time (min)	Area (mAu*s)	Height (mAu)	Area (%)
1	PDA 400.02 nm	28.340	380585	9141	49.39
2	PDA 400.02 nm	30.167	389922	9065	50.61

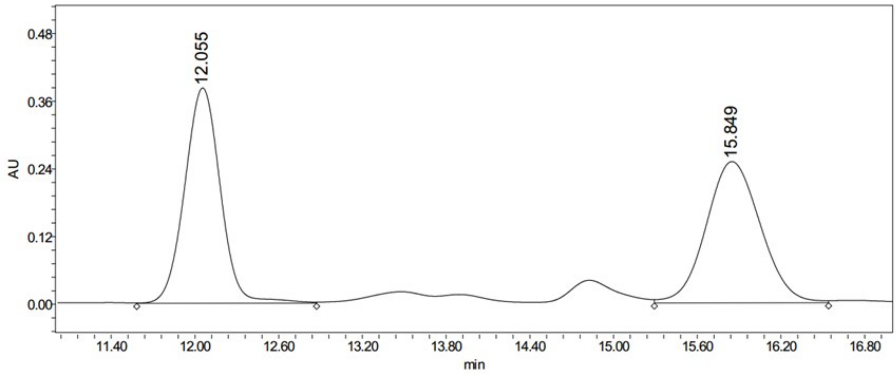

Figure S45. HPLC chromatogram of **6b** on a CHIRALPAK chiral-NR column (Φ = 0.46 cm) at ambient conditions using a mixture solution of cyclohexane and isopropanol (1:1 in volume) as eluent (flow rate 0.5 mL/min).

Table S2. The chiral HPLC chromatographic data of **6b** on a CHIRALPAK chiral-NR column (Φ = 0.46 cm) at ambient conditions

Peak	Processed channel	Ret. Time (min)	Area (mAu*s)	Height (mAu)	Area (%)
1	PDA 400.02 nm	12.055	6793359	381593	50.02
2	PDA 400.02 nm	15.849	6786911	250502	49.98

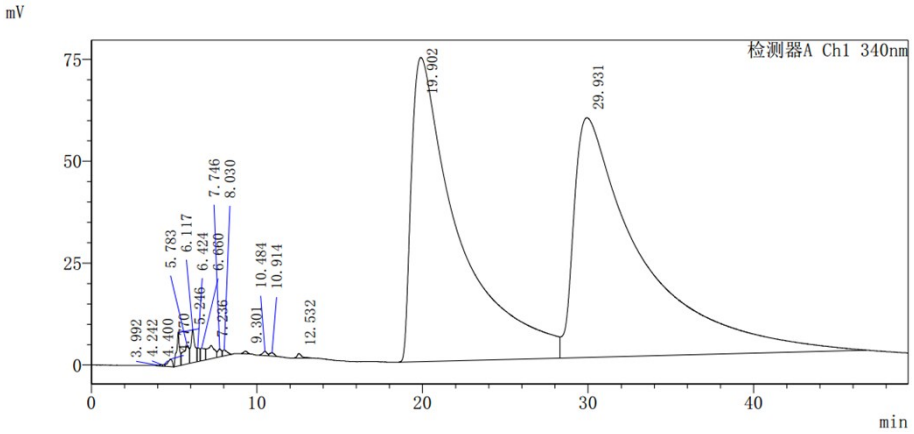

Figure S46. HPLC chromatogram of **1a** on a SHIMADZU-GL INERTSIL chiral- preparation column (Φ = 0.50 cm) at ambient conditions using a mixture solution of cyclohexane and ethyl acetate (2:3 in volume) as eluent (flow rate 0.7 mL/min).

Table S3. The chiral HPLC chromatographic data of **1a** on a SHIMADZU-GL INERTSIL chiral- preparation column (Φ = 0.50 cm) at ambient conditions

Peak	Processed channel	Ret. Time (min)	Area (mAu*s)	Height (mAu)	Area (%)
1	Ch1 340nm	19.902	14794683	74646	46.93
2	Ch1 340nm	29.931	16732072	58839	53.07

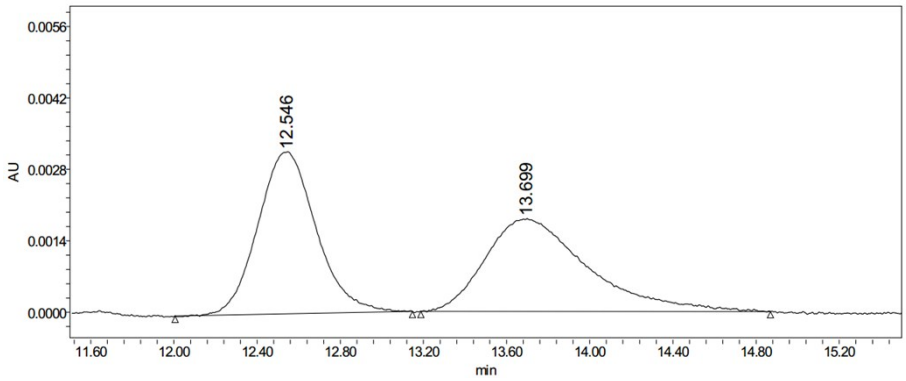

Figure S47. HPLC chromatogram of **1b** on a CHIRALPAK chiral-NR column (Φ = 0.46 cm) at ambient conditions using a mixture solution of cyclohexane and isopropanol (4:1 in volume) as eluent (flow rate 0.5 mL/min).

Table S4. The chiral HPLC chromatographic data of **1b** on a CHIRALPAK chiral-NR column (Φ = 0.46 cm) at ambient conditions

Peak	Processed channel	Ret. Time (min)	Area (mAu*s)	Height (mAu)	Area (%)
1	PDA 400.02 nm	12.546	61940	3176	50.03
2	PDA 400.02 nm	13.699	61866	1814	49.97

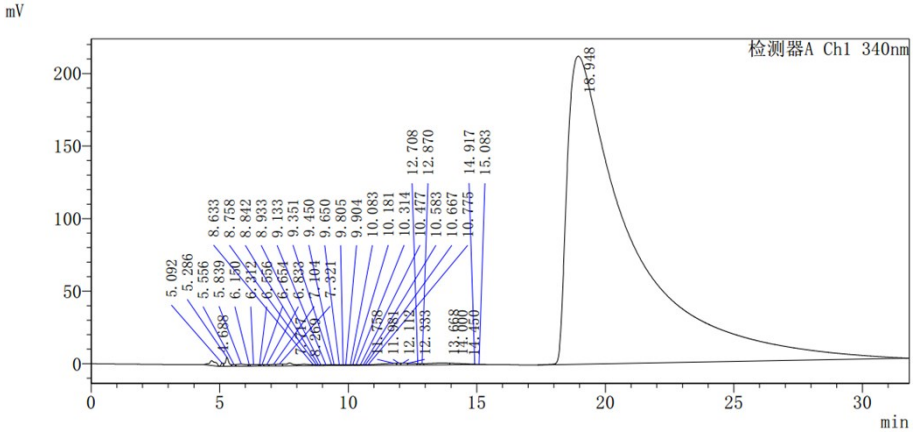

Figure S48. HPLC chromatogram of **1a-1** on a SHIMADZU-GL INERTSIL chiral- preparation column (Φ = 0.50 cm) at ambient conditions using a mixture solution of cyclohexane and ethyl acetate (2:3 in volume) as eluent (flow rate 0.7 mL/min).

Table S5. The chiral HPLC chromatographic data of **1a-1** on a SHIMADZU-GL INERTSIL chiral- preparation column (Φ = 0.50 cm) at ambient conditions

Peak	Processed channel	Ret. Time (min)	Area (mAu*s)	Height (mAu)	Area (%)
1	Ch1 340nm	18.948	36925211	212348	98.29
2	Ch1 340nm	29.931	642434	4394	1.71

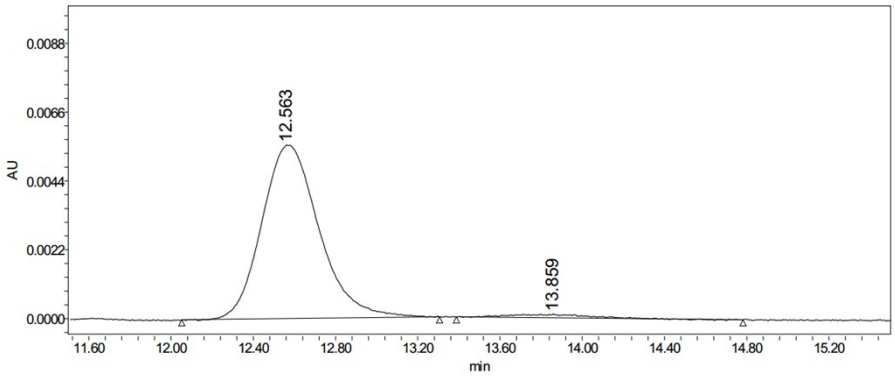

Figure S49. HPLC chromatogram of **1b-1** on a CHIRALPAK chiral-NR column (Φ = 0.46 cm) at ambient conditions using a mixture solution of cyclohexane and isopropanol (4:1 in volume) as eluent (flow rate 0.5 mL/min).

Table S6. The chiral HPLC chromatographic data of **1b-1** on a CHIRALPAK chiral-NR column (Φ = 0.46 cm) at ambient conditions

Peak	Processed channel	Ret. Time (min)	Area (mAu*s)	Height (mAu)	Area (%)
1	PDA 400.02 nm	12.563	107127	5545	97.24
2	PDA 400.02 nm	13.859	3044	121	2.76

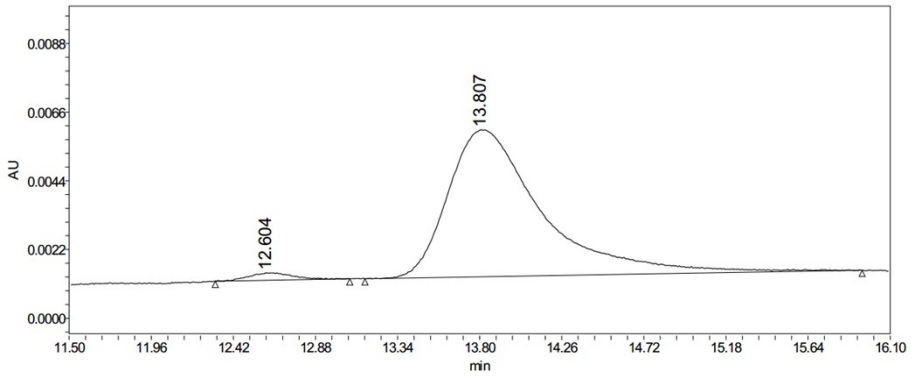

Figure S50. HPLC chromatogram of **1b-2** on a CHIRALPAK chiral-NR column (Φ = 0.46 cm) at ambient conditions using a mixture solution of cyclohexane and isopropanol (4:1 in volume) as eluent (flow rate 0.5 mL/min).

Table S7. The chiral HPLC chromatographic data of **1b-2** on a CHIRALPAK chiral-NR column (Φ = 0.46 cm) at ambient conditions

Peak	Processed channel	Ret. Time (min)	Area (mAu*s)	Height (mAu)	Area (%)
1	PDA 400.02 nm	12.604	4033	237	2.29
2	PDA 400.02 nm	13.807	172049	4706	97.71

5. Absorption absorption, fluorescence and circular dichroism spectral measurements

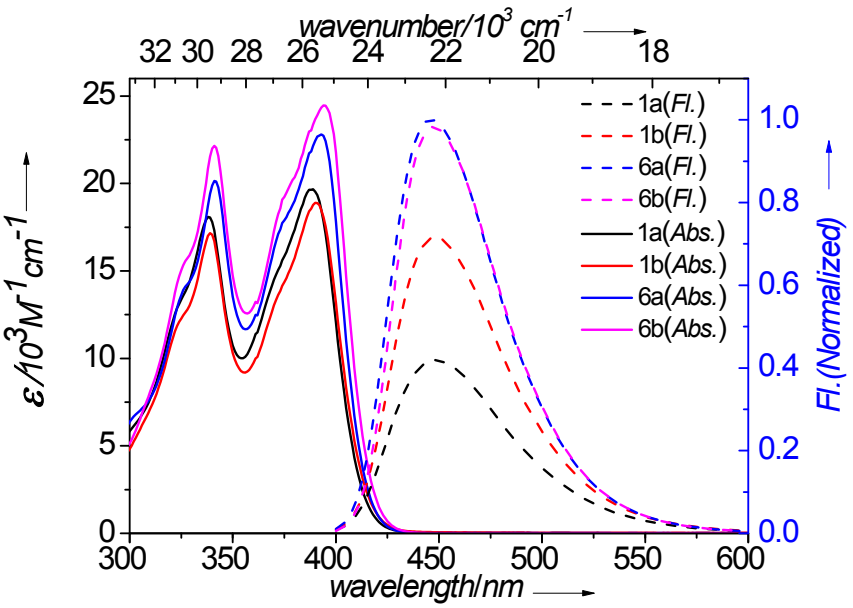

Figure S51. Absorption absorption (solid lines) and fluorescence spectra (dashed lines) of **1a-1b** and their methylated **6a-6b**; All spectra were measured for dilute solutions (10^{-5} M) in ethyl acetate at 298 K, and the fluorescence intensities have been normalized with the strongest emission intensity of **6a**.

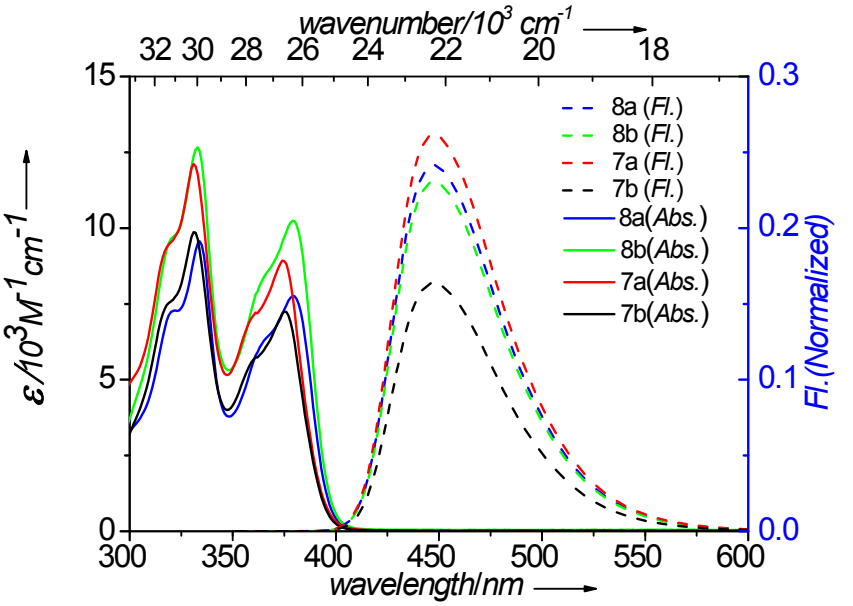

Figure S52. Absorption absorption (solid lines) and fluorescence spectra (dashed lines) of **7a-7b** and their methylated **8a-8b**; All spectra were measured for dilute solutions (10^{-5} M) in ethyl acetate at 298 K, and the fluorescence intensities have been normalized with the strongest emission intensity of **7a**.

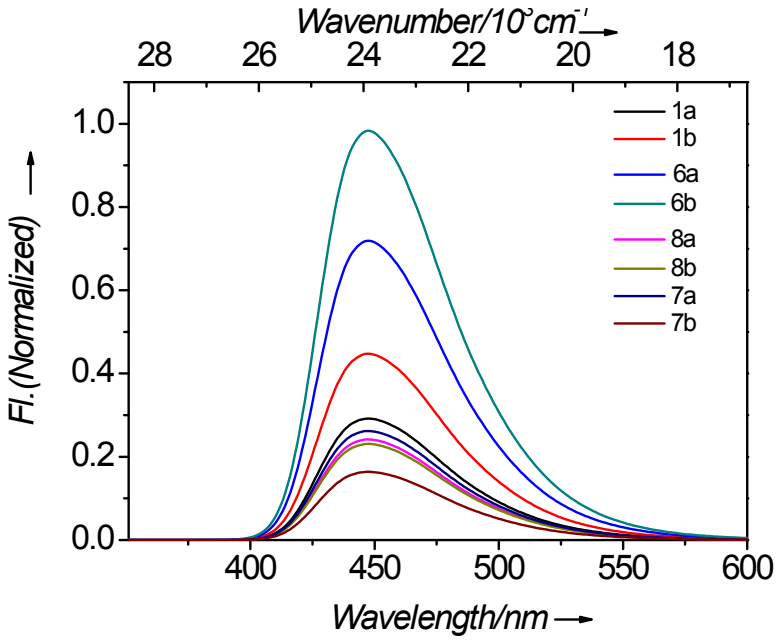

Figure S53. The fluorescence spectral of **1a-1b, 6a-6b, 8a-8b** and **7a-7b** in EA solutions

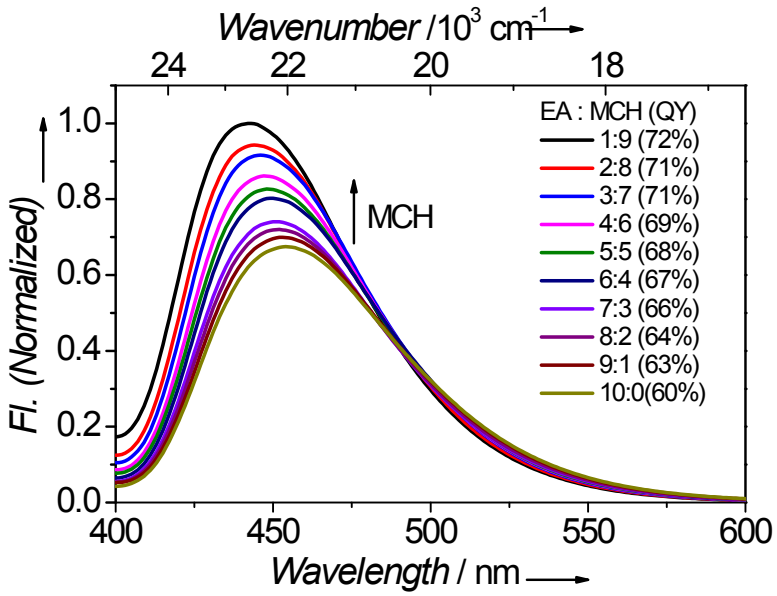

Figure S54. The fluorescence spectral changes of **6a** in EA solutions with the increasing of MCH fractions; for clarity, the fluorescence intensities have been normalized with the strongest emissions in EA-MCH mixture with a ratio of 1: 9.

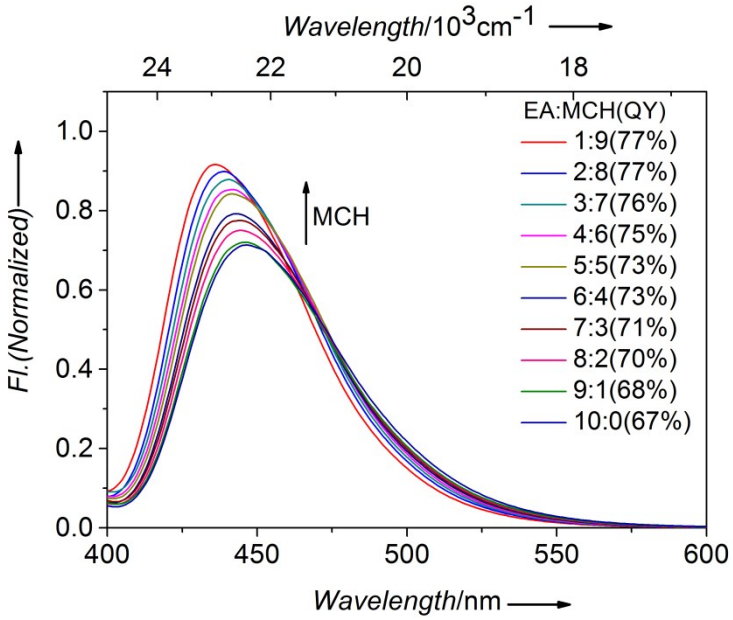

Figure S55. The fluorescence spectral changes of **6b** in EA solutions with the increasing of MCH fractions; for clarity, the fluorescence intensities have been normalized with the strongest emissions in EA-MCH mixture with a ratio of 1: 9.

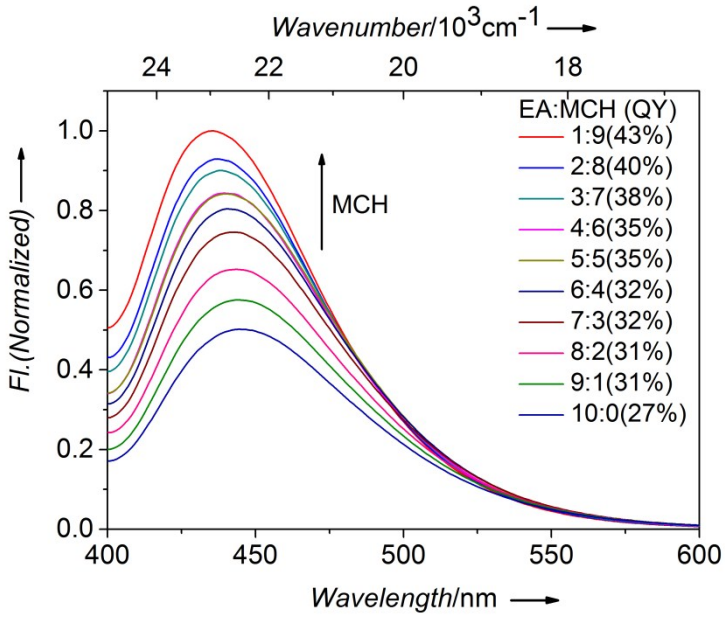

Figure S56. The fluorescence spectral changes of **1a** in EA solutions with the increasing of MCH fractions; for clarity, the fluorescence intensities have been normalized with the strongest emissions in EA-MCH mixture with a ratio of 1: 9.

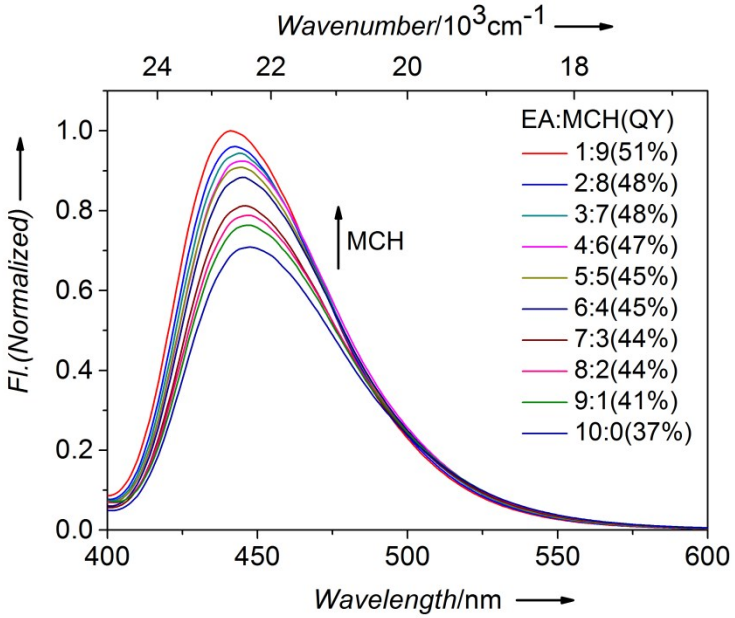

Figure S57. The fluorescence spectral changes of **1b** in EA solutions with the increasing of MCH fractions; for clarity, the fluorescence intensities have been normalized with the strongest emissions in EA-MCH mixture with a ratio of 1: 9.

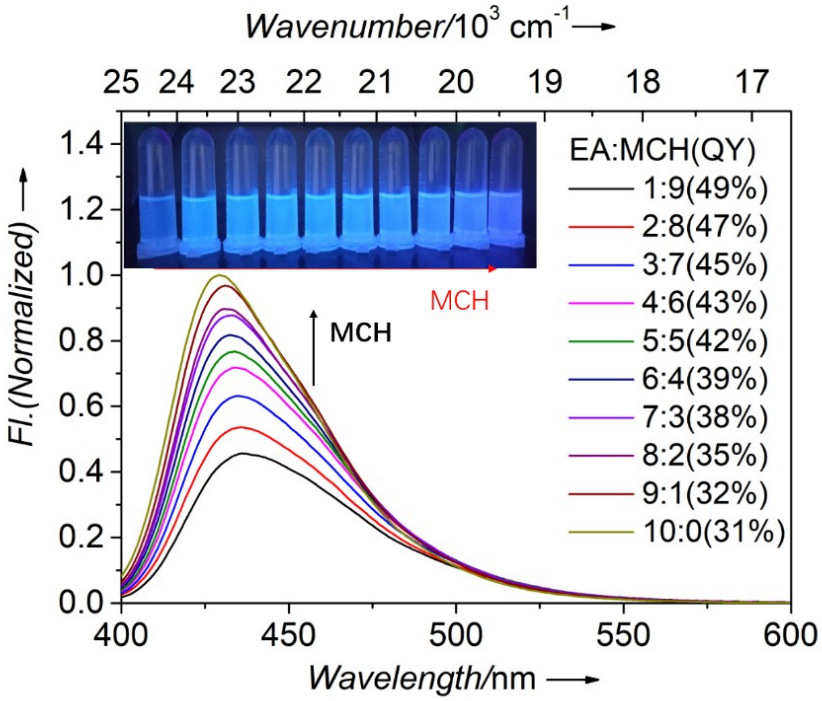

Figure S58. The fluorescence spectral changes of **R-1a** in EA solutions with the increasing of MCH fractions; for clarity, the fluorescence intensities have been normalized with the strongest emissions in EA-MCH mixture with a ratio of 1: 9.

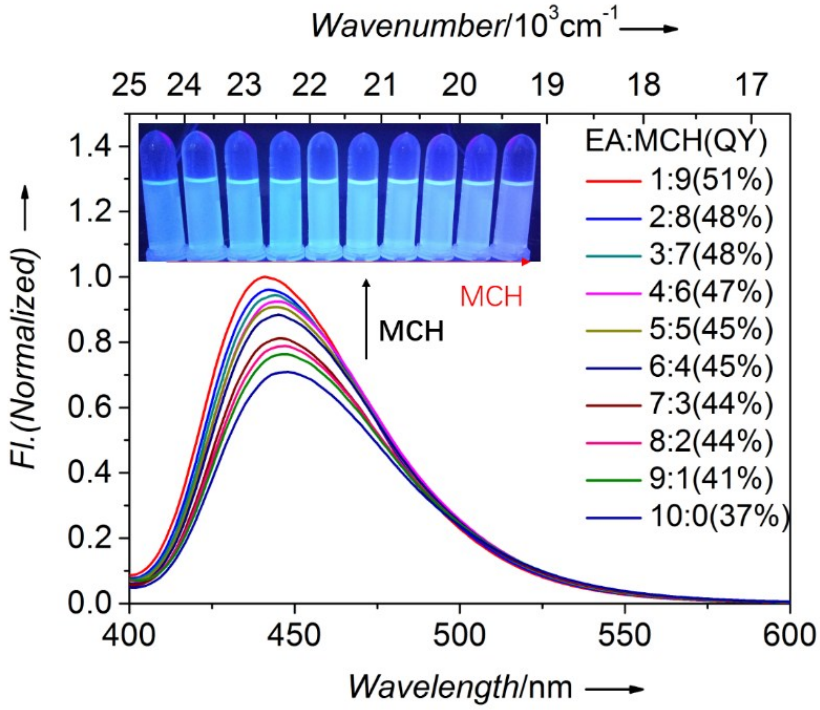

Figure S59. The fluorescence spectral changes of **1b** in EA solutions with the increasing of MCH fractions; for clarity, the fluorescence intensities have been normalized with the strongest emissions in EA-MCH mixture with a ratio of 1: 9

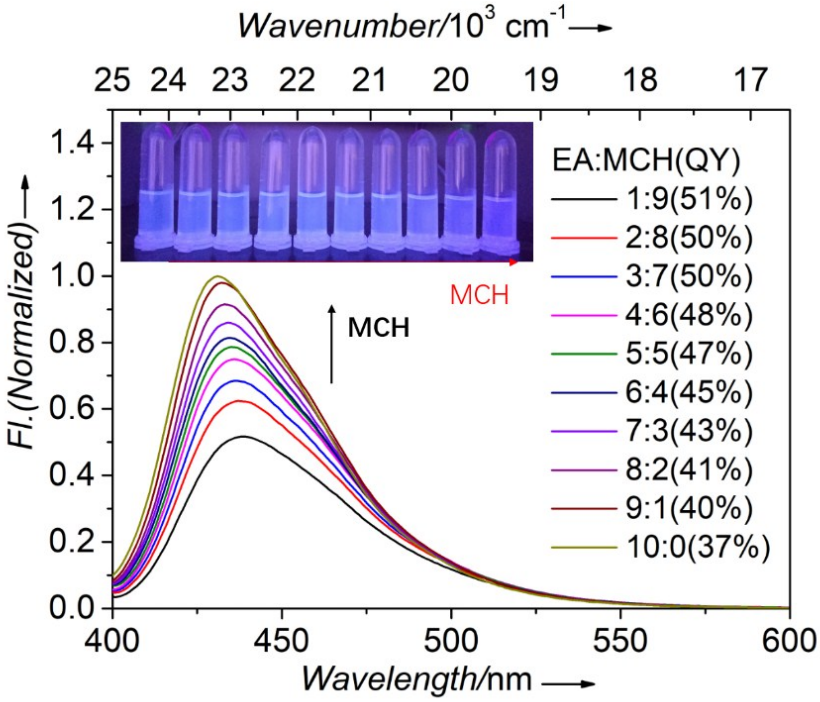

Figure S60. The fluorescence spectral changes of **R-1b** in EA solutions with the increasing of MCH fractions; for clarity, the fluorescence intensities have been normalized with the strongest emissions in EA-MCH mixture with a ratio of 1: 9.

6. Cyclic voltammetry measurements

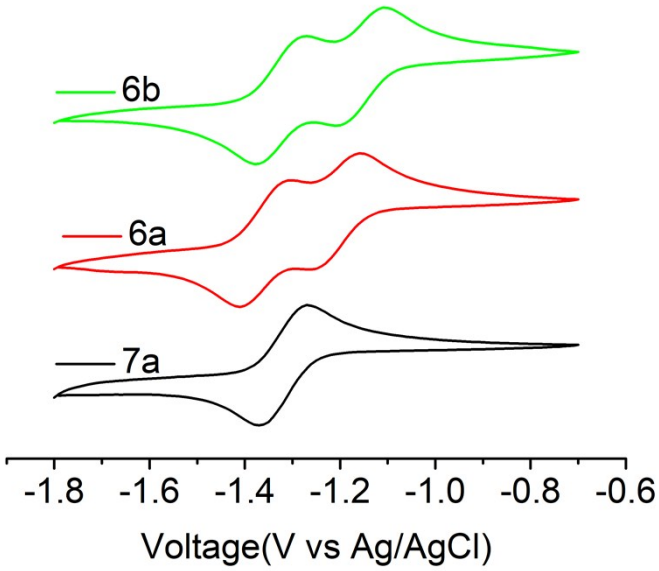

Figure S61. Cyclic voltammetry of **6a**, **6b**, **7a** recorded with a scan rate of 100 mv • s^{-1} at 298K in Ar-purged solvent mixture (ethyl acetate: acetonitrile=5:1) (1mM) using a glassy carbon working electrode and 0.1M $[Bu_4N]^+[PF_6]^-$ as the supporting electrolyte.

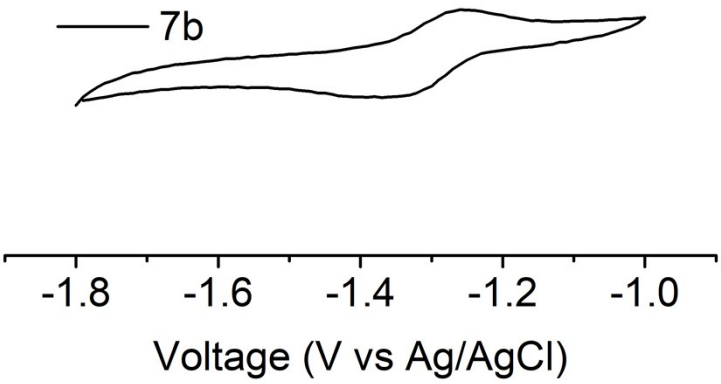

Figure S62. Cyclic voltammetry of **7b** recorded with a scan rate of 100 mv • s^{-1} at 298K in Ar-purged solvent mixture (ethyl acetate: acetonitrile=5:1) (1mM) using a glassy carbon working electrode and 0.1M $[Bu_4N]^+[PF_6]^-$ as the supporting electrolyte.

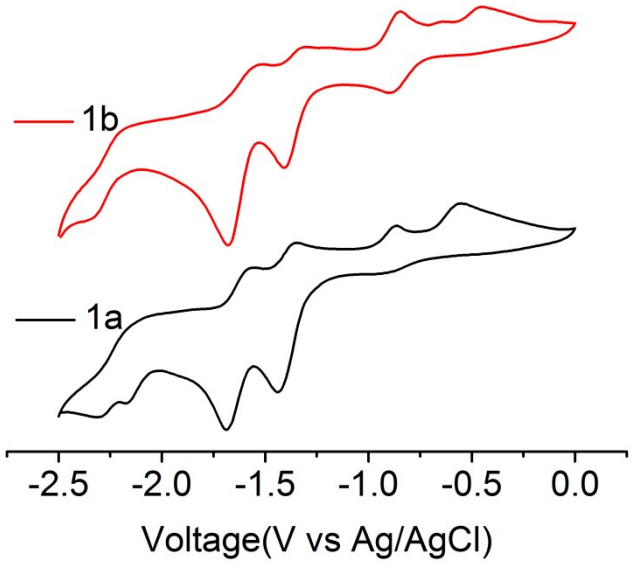

Figure S63. Cyclic voltammetry of **1a** and **1b** recorded with a scan rate of 100 mv • s^{-1} at 298K in Ar-purged solvent mixture (ethyl acetate: acetonitrile=5:1) (1mM) using a glassy carbon working electrode and 0.1M $[Bu_4N]^+[PF_6]^-$ as the supporting electrolyte.

7. Theoretical calculations

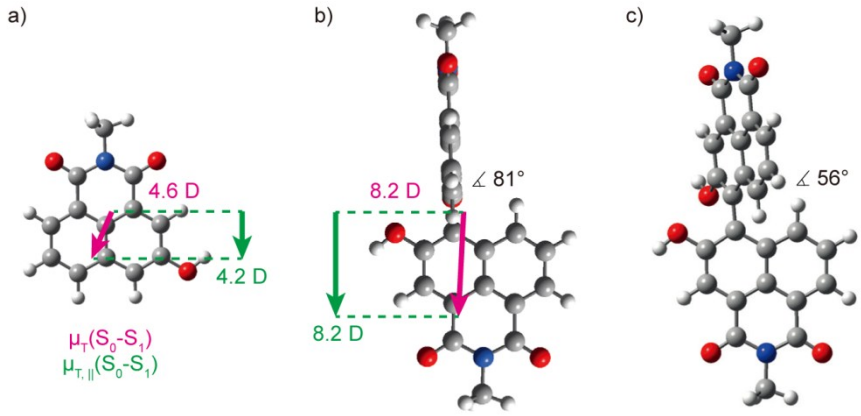

Figure S64. a) Optimized structure of the compound **8** model in the electronic ground state. b) Optimized structure of the compound **1** model in the electronic ground state. c) Optimized structure of the compound 1 model in the electronically excited S1 state. In a) and b), the S0-S1 transition dipole moments (pink) are plotted as well as their projection on the C-C connection axis of the NI units (green)

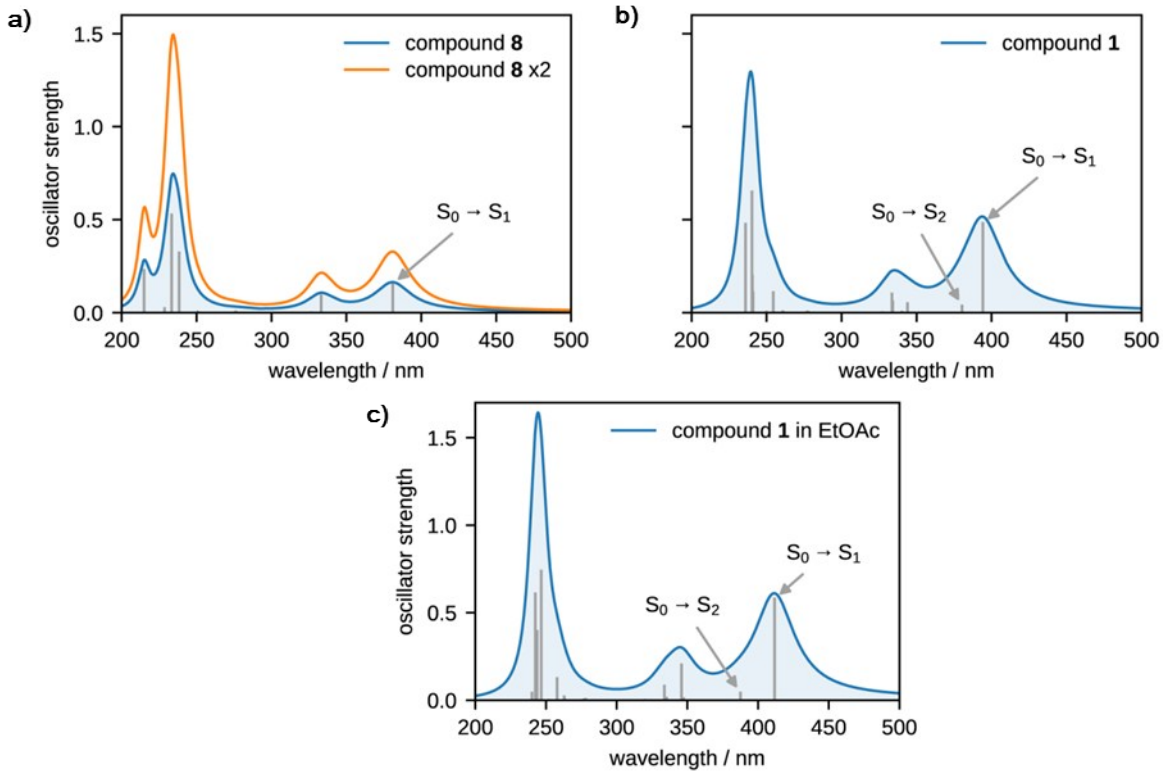

Figure S65. Calculated absorption spectra for a) compound **8** and b) compound **1** in vacuum , as well as c) for compound **1** with an implicit solvation model of ethyl acetate. For better comparability, the spectrum of **8** is also depicted multiplied by a factor of 2.

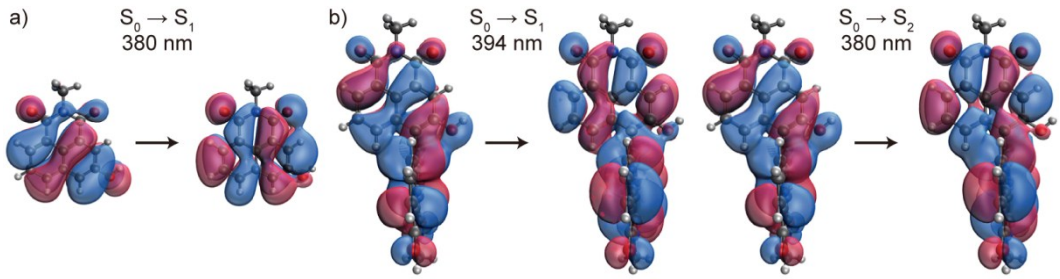

Figure S66. Natural transition orbitals for the lowest electronic transitions in a) compound **8** and b) compound **1** models.

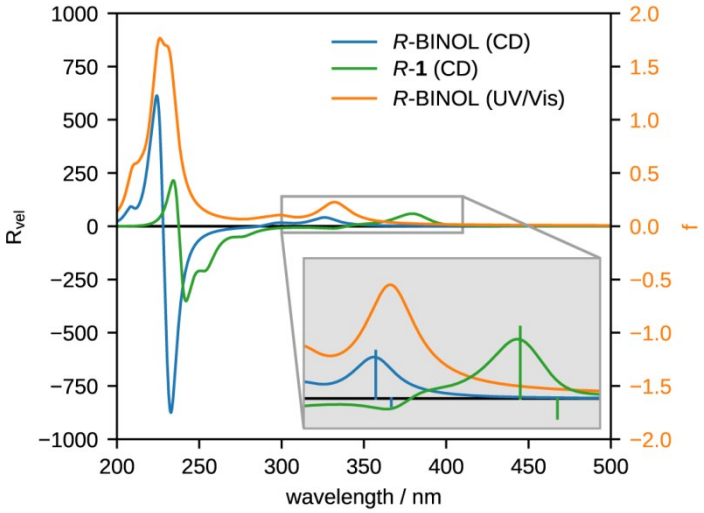

Figure S67. Calculated CD spectra of ***R*-1 a**nd R-BINOL and absorption spectrum of *R*-BINOL. In the zoomed inset, the rotatory strengths for the lowest two vertical transitions are visualized. The spectra have been calculated and convoluted according to the methods section in the main paper.

8. Methanol-water system luminescence measurements

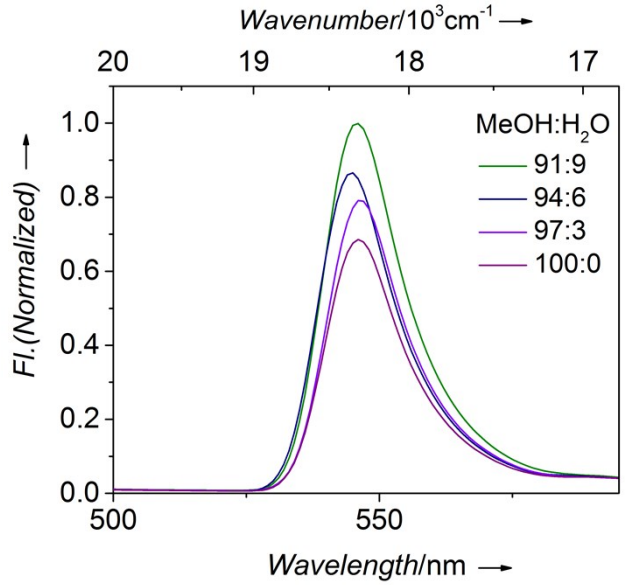

Figure S68. The fluorescence spectral changes of **1a** in CH_3OH solutions with the increasing of H_2O fractions; for clarity, the fluorescence intensities have been normalized in CH_3OH - H_2O mixture with a ratio of 91: 9.

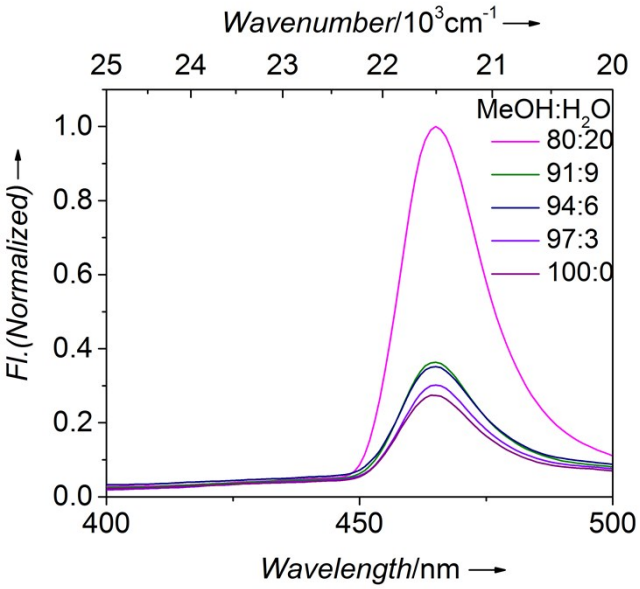

Figure S69. The fluorescence spectral changes of **6a** in CH_3OH solutions with the increasing of H_2O fractions; for clarity, the fluorescence intensities have been normalized in CH_3OH - H_2O mixture with a ratio of 4 : 1.

9. Luminescence lifetime measurements

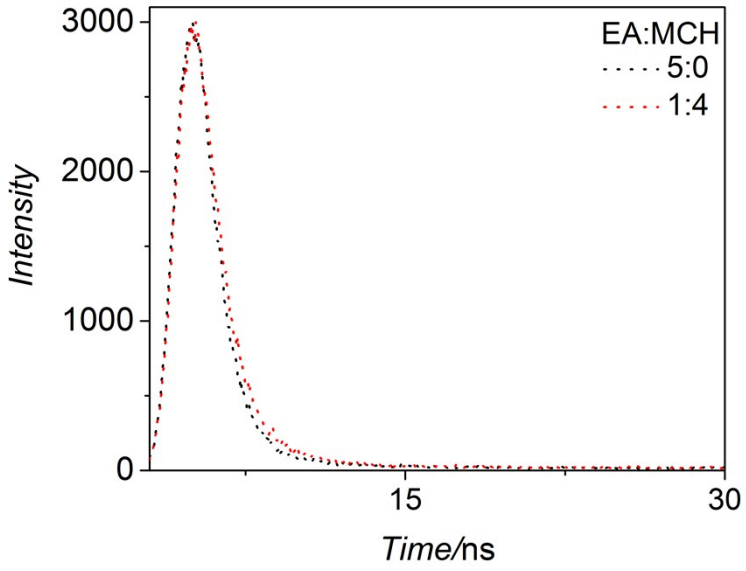

Figure S70. The luminescence lifetime spectra of **1a** at 3×10^{-3} M in the solvent of EA (black dash line) and the mixture of EA-MCH (1:4).

The sample in EA (black dash line) with the lifetime fitting formula:

$$R(t) = 2119.44e^{-t/1.04} + 66.85e^{-t/5.94}$$

$$x^2 = 1.173$$

$t_{(5:0)}$=1.79 ns

The sample in the mixture of 80 % MCH (red dash line) with the lifetime fitting formula:

$$R(t) = 2250.90e^{-t/1.22} + 54.76e^{-t/7.69}$$

$$x^2 = 1.200$$

$t_{(1:4)}$=2.08 ns

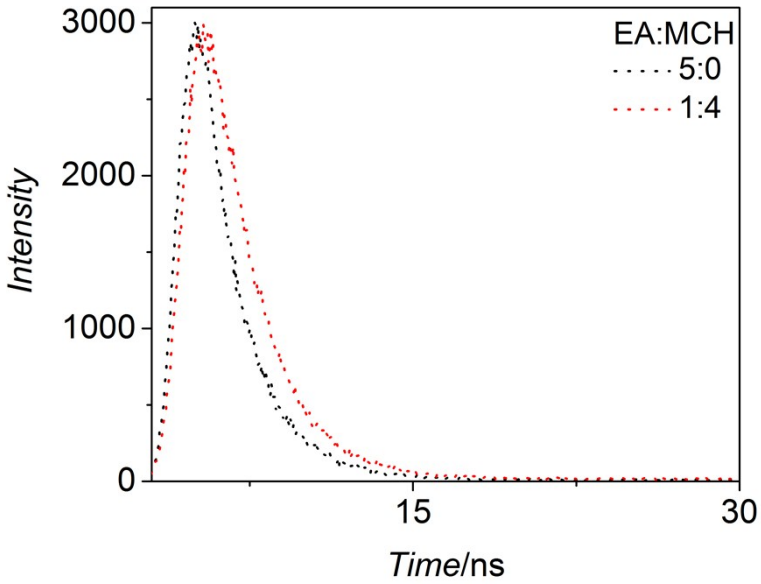

Figure S71. The luminescence lifetime spectra of **1b** at 3×10^{-3} M in the solvent of EA (black dash line) and the mixture of EA-MCH (1:4).

The sample in EA (black dash line) with the lifetime fitting formula:

$$R(t) = 3245.54e^{-t/2.01}$$

$$x^2 = 1.283$$

$t_{(5:0)}$=2.01 ns

The sample in the mixture of 80 % MCH (red dash line) with the lifetime fitting formula:

$$R(t) = 2528.91e^{-t/2.19}$$

$$x^2 = 1.194$$

$t_{(1:4)}$=2.19 ns

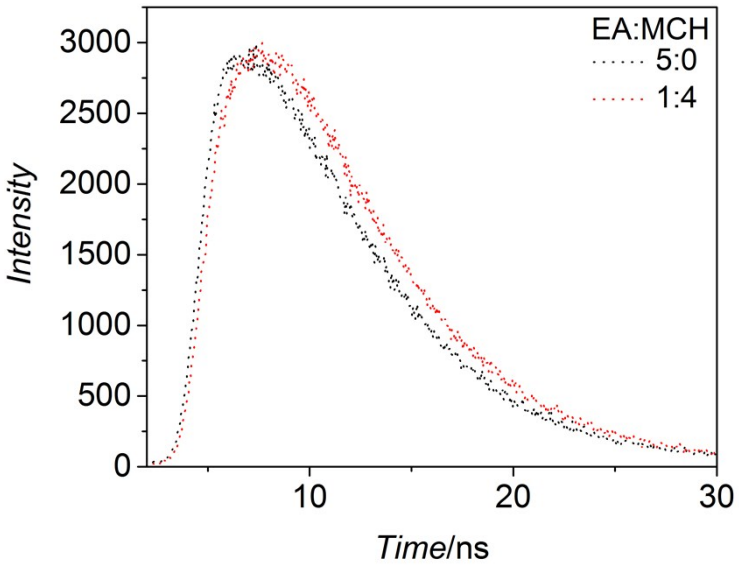

Figure S72. The luminescence lifetime spectra of **6a** at 3×10^{-3} M in the solvent of EA (black dash line) and the mixture of EA-MCH (1:4).

The sample in EA (black dash line) with the lifetime fitting formula:

$$R(t) = 2711.809e^{-t/4.2172}$$

$$x^2 = 1.256$$

$t_{(5:0)}$=4.2172 ns

The sample in the mixture of 80 % MCH (red dash line) with the lifetime fitting formula:

$$R(t) = 1153.44e^{-t/5.2874}$$

$$x^2 = 1.009$$

$t_{(1:4)}$=5.2874 ns

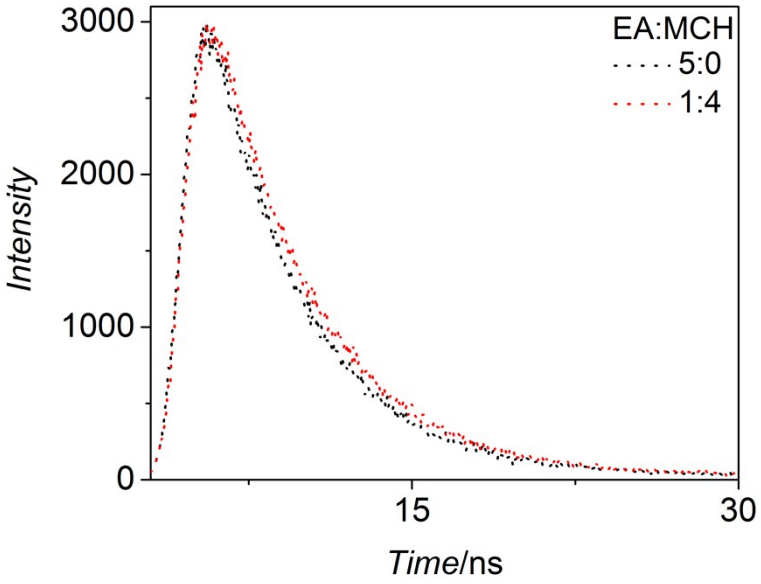

Figure S73. The luminescence lifetime spectra of **6b** at 3×10^{-3} M in the solvent of EA (black dash line) and the mixture of EA-MCH (1:4).

The sample in EA (black dash line) with the lifetime fitting formula:

$$R(t) = 2794.82e^{-t/4.32}$$

$$x^2 = 1.049$$

$t_{(5:0)}$=4.32 ns

The sample in the mixture of 80 % MCH (red dash line) with the lifetime fitting formula:

$$R(t) = 3032.21e^{-t/4.56}$$

$$x^2 = 1.213$$

$t_{(1:4)}$=4.56 ns

10. References

[S1] O.V. Dolomanov, L.J. Bourhis, R.J. Gildea, J.A.K. Howard, H. Puschmann. *J. Appl. Cryst*, **2009**, 42, 339-341.

[S2] G. Sheldrick, *Acta Crystallogr*, **2008**, *A64*, 112-122.

[S3] A. L. Spek*, J. Appl. Cryst.*, **2003***, 36,* 7-13.